FORMATION OF $SRTiO_3[TiO_2]$ CERAMIC COMPOSITES AT LOW TEMPERATURES

A Thesis Submitted to
the Graduate School of Engineering and Sciences of
İzmir Institute of Technology
in Partial Fulfillment of the Requirements for the Degree of

MASTER OF SCIENCE

in Materials Science and Engineering

by
Esin KARATAŞ

July 2021
İZMİR

ACKNOWLEDGMENTS

Firstly, I would like to thank to members of the thesis committee, Prof. Dr. Ali Aydın GÖKTAŞ and Assoc. Prof. Fatih TOPTAN for their valuable and guiding comments and suggestions.

I also would like to thank the members of our research group including Levent Karacasulu, Cerem Pişkin, Tuğçe Semerci, Öykü İçin, and Ezgi Oğur for their friendship and support.

I would like to thank my older sister Gülebru, my mother and father for their support during my MSc and my all life. I would also like to express my gratitude to my dear Oğuz, who is with me in every difficulty I face and always believes in me. They have consistently supported and encouraged me to follow my dreams.

I wish to thank all my family and friends for their supports. I dedicate this thesis to my lovely family.

ABSTRACT

FORMATION OF $SrTiO_3[TiO_2]$ CERAMIC COMPOSITES AT LOW TEMPERATURES

Strontium titanate ceramics are materials belonging to the perovskite material group with the formula ABO_3. Strontium titanate ceramics have been a preferred material in many areas, such as the electroceramics industry, due to its high dielectric constant and high chemical stability and generally produced by manufacturing processes such as solid-state synthesis, hydrothermal method, and sol-gel. $SrTiO_3$ ceramics have been produced in the literature with different temperatures, times, and starting materials. For ceramic products, a sintering step is required after the powder production step. Traditional sintering methods, which have been used for many years, are used to densify powders with high temperatures. Recently developed low-temperature densification methods enable the sintering process to be carried out at relatively lower temperatures. For this purpose, in this thesis, $SrTiO_3$-TiO_2 ceramic composites were produced at different reaction temperatures and times using the rHLPD method, which combines powder production and sintering steps in a single process. In the studies, the reaction temperature, time, and the effect of adding mineralizer to the prepared solution for the hydrothermal reaction on the final product were investigated. The aim of the thesis is to produce $SrTiO_3$ from TiO_2 green body using the rHLPD method. In addition, the production of $SrTiO_3$-TiO_2 ceramic composites with as high mole conversion and relative density values as possible was targeted with different parameters such as reaction temperature, reaction time, and addition of NaOH to the solution. As a result of the studies carried out with different parameters, $SrTiO_3$-TiO_2 ceramic composites with a final relative density value of approximately 81 % were produced.

Consequently, in the XRD and Rietveld analysis, it was seen that the main phase was $SrTiO_3$. In addition, there was a TiO_2 phase in the structure. Finally, the $SrCO_3$ phase was not detected in the structure.

ÖZET

DÜŞÜK SICAKLIKLARDA $SrTiO_3[TiO_2]$ SERAMİK KOMPOZİTLERİN OLUŞUMU

Stronsiyum titanat seramikler, ABO_3 formülüne sahip perovskit malzemeler sınıfına ait bir malzemedir. Stronsiyum titanat seramikler, yüksek dielektrik sabiti, yüksek kimyasal kararlılığı gibi özelliklerinden dolayı elektroseramik endüstrisi gibi birçok alanda tercih edilen bir malzeme olmuştur ve genellikle katı hal sentezi, hidrotermal yöntem ve sol jel gibi üretim süreçleriyle üretilmektedir. Stronsiyum titanat seramikleri, literatürde çok farklı sıcaklık, süre ve başlangıç malzemeleri ile üretilmiştir. Seramik ürünler için, toz üretim aşamasının ardından sinterleme adımı gerekmektedir. Uzun yıllardır kullanılan geleneksel sinterleme yöntemleri, üretilen tozların yüksek sıcaklık ile yoğunlaştırılmasıdır. Yeni geliştirilen düşük sıcaklık yoğunlaştırma yöntemleri ise nispeten daha düşük sıcaklıklarda sinterleme işleminin gerçekleştirilmesi sağlamaktadır. Bu amaçla bu tezde toz üretim ve sinterleme adımını tek bir işlemde birleştiren rHLPD yöntemi kullanılarak farklı reaksiyon sıcaklıkları ve reaksiyon sürelerinde $SrTiO_3$- TiO_2 seramik kompozitleri üretilmiştir. Yapılan çalışmalarda reaksiyon sıcaklığı, süresi ve hidrotermal reaksiyon için hazırlanan çözeltiye mineralizer eklenmesinin son ürün üzerindeki etkisi incelenmiştir. Bununla birlikte, tezin amacı rHLPD yöntemi kullanılarak TiO_2 yeşil gövdesinden $SrTiO_3$ üretimini gerçekleştirmektir. Reaksiyon sıcaklığı, reaksiyon süresi ve çözeltiye eklenen NaOH konsantrasyonu gibi farklı parametreler ile olabildiğince yüksek mol dönüşümüne ve relatif yoğunluk değerine sahip $SrTiO_3$-TiO_2 seramik kompozitlerinin üretilmesidir. Farklı parametreler ile gerçekleştirilen çalışmalar sonucu, yaklaşık %81 final relatif yoğunluk değerine sahip $SrTiO_3$-TiO_2 seramik kompozitleri üretilmiştir.

Yapılan XRD ve Rietveld analizleri sonucunda ana fazın $SrTiO_3$ olduğu görülmüştür. Bunun yanında yapıda TiO_2 fazı gözlemlenmiş olup, $SrCO_3$ fazı yapı içinde tespit edilmemiştir.

TABLE OF CONTENTS

LIST OF FIGURES

Figure **Page**

Figure **Page**

LIST OF TABLES

Table **Page**

CHAPTER 1

INTRODUCTION & MOTIVATION

Metal oxides with the chemical formula ABO_3 are commonly known as perovskites. These materials have become preferred in many areas due to their specific properties. Strontium titanate, $SrTiO_3$, a metal oxide composed of Sr, Ti, and oxygen, is a ceramic with a perovskite structure. Strontium titanate ceramics, which have a cubic crystal structure at room temperature, are used in many fields, such as electroceramics.

It is necessary first to produce ceramic powder to produce ceramic products. This step is carried out by different powder production methods such as solid-state synthesis, sol-gel, and hydrothermal. Production methods have different effects on the final properties of the powder produced.

Next, a process called sintering is needed to transform powder components into ceramic products. During the sintering step, the powder components reduce their pores, becoming a denser monolith. In nature, these processes have been going on spontaneously for thousands of years. Many processes, such as lithification involve the compression of free particles to become dense with a reduction in porosity. While these processes can occur under very high temperatures and pressure in nature, it is impossible to reach these pressures in the industry. These processes, which take place over a long time in nature, must occur in shorter periods.[1] In traditional sintering methods, powder components are condensed at high temperatures and transformed into ceramic products.

Due to the changing world conditions, it has recently become essential to reduce the carbon footprint and protect nature by minimizing energy consumption. In this direction, scientists have developed new technologies that enable the production of ceramic products in one step by combining the powder synthesis and sintering steps at lower temperatures. Unlike conventional sintering methods, densification is carried out at lower temperatures in low-temperature densification methods. The rHLPD method is one of these methods[1] The aim and motivation of this thesis are to densify $SrTiO_3$ ceramics with the rHLPD method in one step without the powder production step at lower temperatures.

1.1. Structure and Scope

In the first chapter, the introduction, general information about the thesis is given. In chapter 2, information about perovskite structures and powder production methods and the production of strontium titanate ceramics will be given, and the studies will be summarized. Following the powder production methods, traditional sintering and low-temperature densification methods will be included. Finally, brief information about the properties and application areas of strontium titanate ceramics will be given. Chapter 3 will show the experimental procedure of the work done throughout the thesis. The study results and discussion will be illustrated in chapter 4, and finally, a brief conclusion about the study will be given in chapter 5.

CHAPTER 2

LITERATURE REVIEW

2.1. Perovskite Materials

Metal oxides with the chemical formula ABO_3 are commonly known as perovskites.[2] A is mostly a group I or II elements, and B is the transition metal. In 1839, the $CaTiO_3$ mineral discovered by Gustav Rose in the Ural Mountains was named after the Russian mineralogist Lev Perovskite, materials with a crystal structure similar to calcium titanate were named perovskite.[3]

ABX_3 is known as the general formula of perovskite materials. A perovskite structure is defined as a cubic structure containing an A-site atom in the center of the cube, a B-site atom at the corners of the cube, and X atoms in the cell edge centers. The atom represented by X is usually O or F atoms (Figure 2.1.).[4]

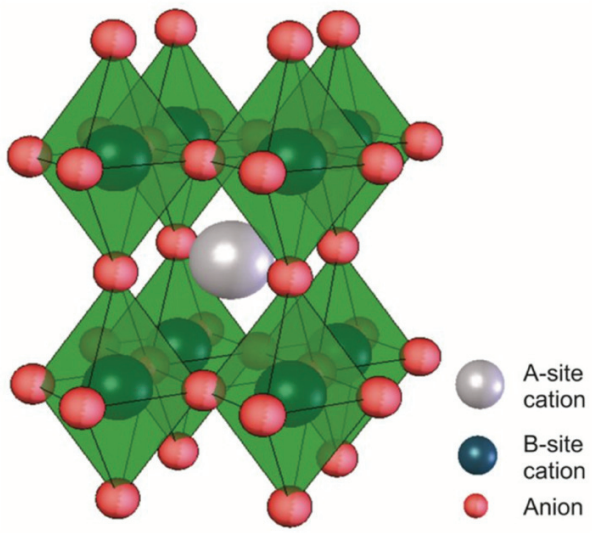

Figure 2.1. A representative cubic perovskite structure
(Source: Nikonov, 2018).[5]

Perovskite ferroelectric materials are an advanced class of electronic materials that have an electric dipole moment of their own in a specific temperature range.[6] Ferroelectric materials can reverse the spontaneous polarization formed by the applied electric field.[4] A characteristic property of ferroelectric materials is that they have a phase transition temperature called T_c Curie temperature. Curie temperature can be expressed as the paraelectric-ferroelectric phase transition temperature. Below the Curie temperature, a ferroelectric crystal undergoes a phase transformation from the ferroelectric phase to the paraelectric phase. The crystal shows ferroelectric properties when it falls below the Curie temperature and loses its ferroelectric properties when it is above the Curie temperature.[7]

There are few perovskite-type materials with ideal cubic structures. This property is available in materials that exhibit ferroelectric behavior thanks to dipoles that occur due to distortions in the cells.[4] Figure 2.2 shows the distortion to which the $BaTiO_3$ lattice is exposed. $BaTiO_3$ no longer exhibits ferroelectric properties, as distortion will disappear when the barium titanate compound is heated above 120°C.[4]

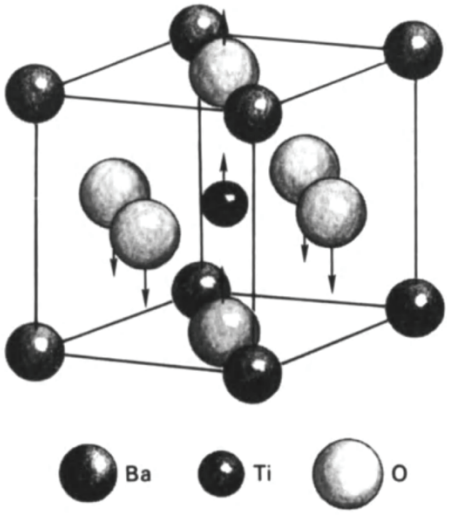

Figure 2.2. The representative barium titanate structure
(Source: Galasso, 2013). [4]

2.2. Strontium Titanate Ceramics ($SrTiO_3$)

Although strontium titanate was first reported in 1935, it was not understood that it had a perovskite structure until 1946.[8] Strontium titanate is an oxide composed of the elements oxygen, titanium, and strontium. $SrTiO_3$ is a paraelectric material with a perovskite structure, widely used for electronic applications and attracted by its potential use for modern electronic devices.[9-11]

At room temperature, strontium titanate is an ideal cubic perovskite with Pm3m space group, lattice parameter a = b = c= 0.3905.[8, 12] If $SrTiO_3$ is cooled from RT, it undergoes from cubic (space group P4mm) phase to tetragonal phase at T_c = 105K (-168.15^{o}C).[11] Temperature changes in perovskite structure easily cause phase changes.[8] Normally, such a phase transition leads to ferroelectricity. However, since $SrTiO_3$ does not show a transition up to 0K, it is included in the paraelectric or incipient ferroelectric group.[13] Strontium titanate is superconductive at low temperatures.[14]

The cubic perovskite crystal structure of $SrTiO_3$ is shown in Figure 2.3. At the edges of the cube, Sr^{2+} (A cation) is located at the cube edge centers with twelve O^{2-} around the large positively charged ions, the smaller Ti^{4+} ions (B-cation) form an octahedral with six O^{2-} ions around the center of the cube.[8]

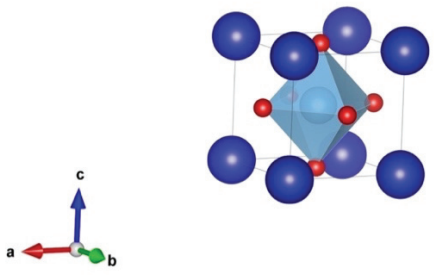

Figure 2.3. The unit cell of the cubic perovskite lattice of strontium titanate ($SrTiO_3$) (Source: Gillani, 2020).[15]

The ideal cubic structure of $SrTiO_3$ can undergo two different changes due to the effect of stress and temperature: ferroelectric type (FE) (Figure 2.4(a)) displacement and antiferrodistortive (AFD) rotation (Figure 2.4(b)). Generally, it is more likely to occur in perovskite materials is determined by the Goldschmidt tolerance factor.[16] Goldschmidt tolerance factor, t, describes cases where different structures are stable.[8] Here, r_A, r_B, and r_o represent the ionic radii of A, B, and oxygen atoms, respectively.[16]

$$t = \frac{r_A + r_O}{\sqrt{2}(r_B + r_O)} \qquad \text{(I)}$$

If t> 1, ferroelectric type displacement occurs in perovskite materials, and they are ferroelectric. Otherwise, if the tolerance factor is less than 1 (t <1), the materials prefer antiferrodistortive rotation. The t value for $SrTiO_3$ is about 1 (t ~1.002). This shows that $SrTiO_3$ can undergo both distortions.[16]

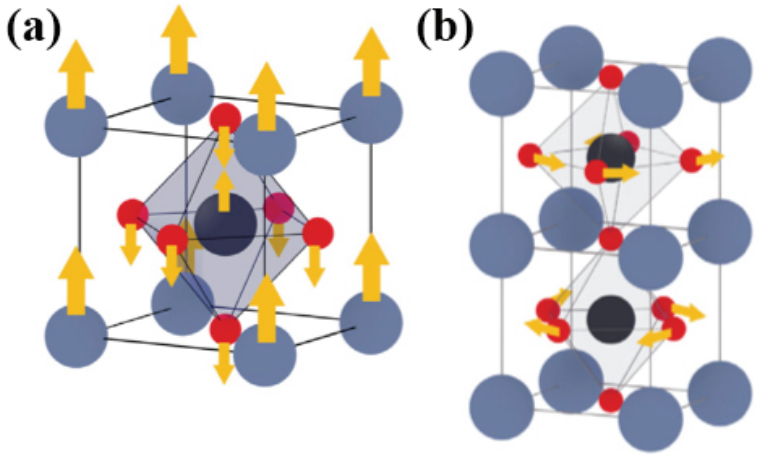

Figure 2.4. Change of the cubic structure, (a) Ferroelectric displacement, and (b) Antiferrodistortive rotation (Source: Pai, 2018).[16]

2.3. Synthesis of Strontium Titanate Ceramic Powders

Strontium titanate ceramic powders can be prepared by various synthesis methods: solid-state synthesis, hydrothermal synthesis, molten salt, and sol-gel methods. Different production methods are effective in the powder produced with different morphology, crystallinity, impurity, particle size, and shape.[13]

2.3.1. Solid-State Synthesis

Among traditional powder preparation methods, solid-state synthesis is the oldest known, easiest, and most used method to produce inorganic solids.[17, 18] The reaction mainly occurs between solid starting materials such as carbonates, hydroxides, and other salts.[19, 20] The starting materials in powder form are mixed for a certain period and then heat-treated at high temperatures in the muffle furnace (T > 1000°C). Figure 2.5 shows the formation mechanism of solid-state synthesis.

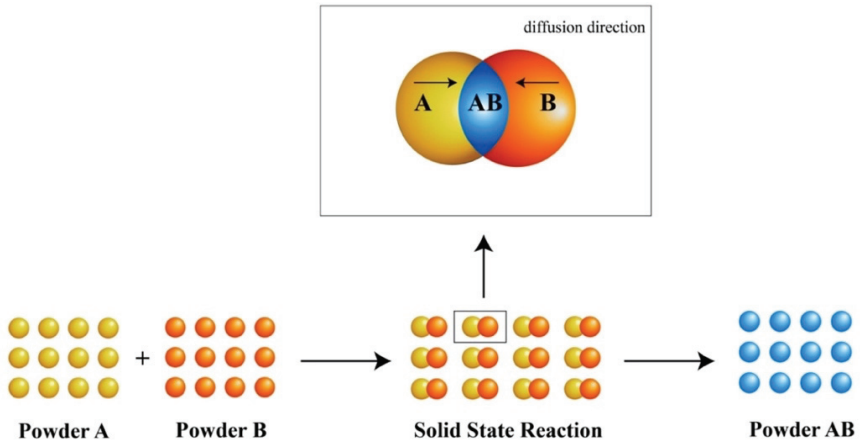

Figure 2.5. Schematic illustration for the solid-state synthesis formation mechanism.[19]

A solid-state reaction involves nucleation of the final product followed by grain growth. The reaction starts at the interface between the two solid phases.[20] The reaction process is relatively slow. Solid-state synthesis is an effective method, although it is easier compared to other ceramic powder preparation methods. The mixing of the powdered particles is crucial for the properties of the final product.[18, 21]

This method, widely used among traditional powder preparation methods, is still highly preferred due to easily accessible and cheap raw materials and uncomplicated process steps.[22]

The production of strontium titanate ceramics by solid-state synthesis, which is one of the most preferred powder production methods, is included in many studies in the literature. In the solid-state synthesis of strontium titanate, the strontium source is usually $SrCO_3$. Calcination and sintering temperature are two important parameters. Calcination temperature in the production of $SrTiO_3$ by solid-state synthesis generally varies between 700°C and 1350°C.[23-28] In addition, the sintering temperature is selected between 1000°C and 1500°C.[17, 25, 26, 29-31]

In the study of Yan et al., the effect of sintering temperature on microstructure and electrical properties was studied. In the study where TiO_2 and $SrCO_3$ were used as starting materials, after mixing the raw materials in stoichiometric proportions, calcination was performed at different temperatures for 10 h. The calcined powders were then pressed into pellets. The obtained pellets were subjected to a sintering process at different temperatures. According to XRD analysis, in sintering at 1000°C, the $SrCO_3$ phase was also seen in the structure in addition to the $SrTiO_3$ phase. Increasing sintering temperature was caused an increase in grain size.[29]

In another study, Liu et al., the effect of three different methods on $SrTiO_3$ synthesis was examined. One of the three methods is solid-state synthesis using $SrCO_3$ and TiO_2 as raw materials. Others are polymeric complex method and milling assistant method. Powders synthesized by solid-state synthesis were calcined at different temperatures and times. According to the results, 800°C-3 h calcination conditions are not sufficient for the pure cubic $SrTiO_3$ phase. On the other hand, when the particle sizes of the powders produced by three different methods are compared, the powders with the largest particle size are produced by solid-state synthesis. The photocatalytic activity of strontium titanate is better in powders produced with the polymeric complex than in solid-state synthesis powders.[32]

In the study of Wang et al., the effect of Sr/Ti molar ratio on microstructure and energy storage properties was studied. Experiments were carried out by changing the Sr/Ti molar ratio between 0.994 and 1.004. After calcination of the produced powders at 1150°C for 2 h, it was made into pellets and sintered at 1440°C for 2 h. In all compositions, the cubic $SrTiO_3$ phase was produced without any secondary phases. When the molar ratio is less than 1, large particle size particles form, small particle size particles occur when the ratio exceeds 1. Among the samples, the highest permittivity value was observed with Sr/Ti: 1.004. The molar ratio of the sample with the highest breaking strength (210 kV/cm) and energy density (0.7 J/cm^3) is Sr/Ti: 0.996.[30]

Table 2.1. Synthesis of strontium titanate ceramic powder by the solid-state method in scientific studies.

Ingredients	**Conditions**	**Produced material(s)**	**Notes**	**Ref.**
TiO_2(rutile), NaCl and $SrCO_3$	Calcination: 700°C for 2 h	$SrTiO_3$	Molar ratio of Sr/Ti=1	24
			Addition of NaCl: nanoparticles at low temperatures	
TiO_2 and $SrCO_3$	Calcination: 1100°C for 2 h	$SrTiO_3$		33
TiO_2 and $SrCO_3$	Calcination: 800-1000°C for 3-5 h	$SrTiO_3$	800°C for 3h is not enough pure $SrTiO_3$	32
TiO_2 and $SrCO_3$	Calcination: 800°C for 2 h	$SrTiO_3$		32
TiO_2 and $SrCO_3$	Calcination: 800-1000-1300°C for 8-10-12 h	$SrTiO_3$	Molar ratio of Sr/Ti=1	28

(Cont. on the next page.)

Tablo 2.1. Cont.

TiO_2 and $SrCO_3$	Calcination: 800-1000- 1200°C for 10 h	$SrTiO_3$ $SrCO_3$		29
TiO_2 and SrC_2O_4	Calcination: 1350°C for 3.5 h	$SrTiO_3$		23
TiO_2 and $SrCO_3$	Calcination: 1150°C for 2 h	$SrTiO_3$	Sr/Ti>1 small grain size Sr/Ti<1 larger grain size	30
TiO_2 and $SrCO_3$	Calcination: 1300°C for 10 h	$SrTiO_3$		31
TiO_2 and $SrCO_3$	Calcination: 1050°C for 6 h	$SrTiO_3$	Molar ratio of Sr/Ti =1/0.997/1.02	34
TiO_2 and $SrCO_3$	Calcination: 1100°C for 15 h	$SrTiO_3$		35
TiO_2 and $SrCO_3$	Calcination: 800°C for 12 h	$SrTiO_3$		25
TiO_2 and $SrCO_3$	Calcination: 900°C for 24 h	$SrTiO_3$		36
TiO_2 and $SrCO_3$	Calcination: 900°C for 12 h	$SrTiO_3$		26
TiO_2 and $SrCO_3$	Calcination: 1000°C for 10 h	$SrTiO_3$		37
TiO_2 and $SrCO_3$	Calcination: 1300°C for 3 h	$SrTiO_3$		38

2.3.2. Sol-gel Method

The sol-gel method is a wet chemical method used for the synthesis of nanomaterials.[39] Sol-gel method makes it possible to produce more homogeneous, narrower particle size distribution and higher purity synthesized powders compared to solid-state reaction.[21, 22]

Figure 2.6 represents the sol-gel formation mechanism. The method consists of sol and gel components. Sol is a colloidal dispersion of nanoscale particles.[40] In the sol-gel method, metal alkoxide and acetylacetone are used as oxide sources, alcohol as a solvent, water as hydrolysis material.[41] Metal compounds in the solvent are undergone hydrolysis and polycondensation at ambient conditions, and then it provides the left formation of finely dispersed nanoparticles.[41, 42] As the reaction continues, the particles bind to each other, turning the sol into a three-dimensional structure called a gel.[40, 41] The resulting gel is named aerogel or xerogel according to different drying conditions.[41]

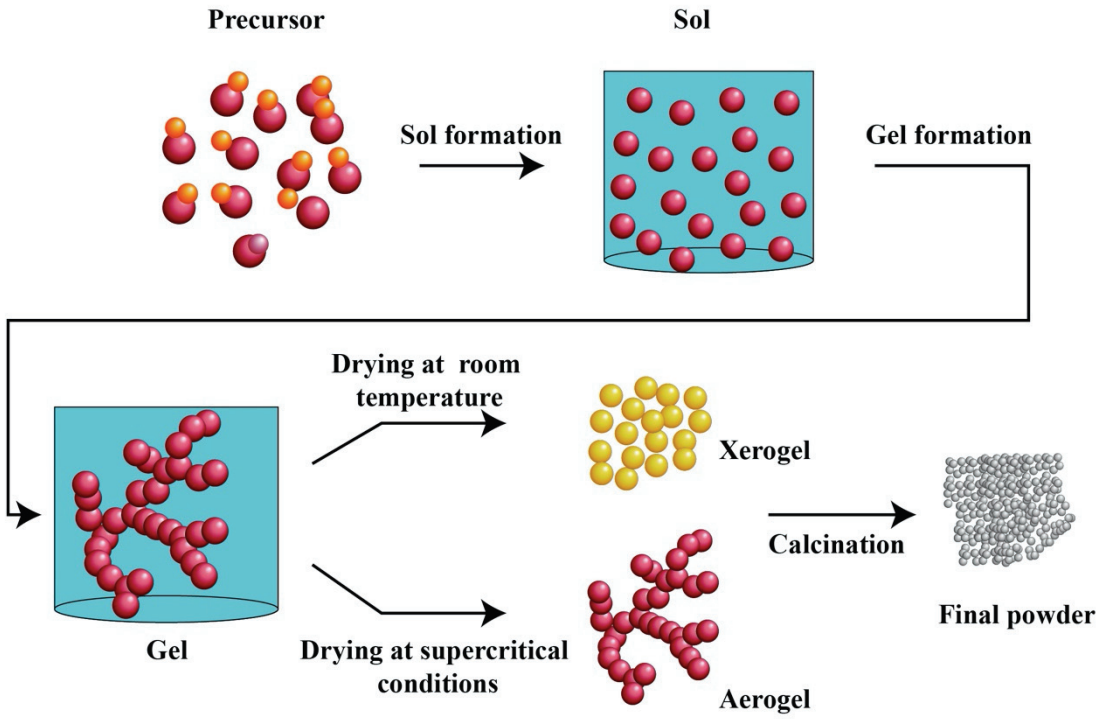

Figure 2.6. Schematic illustration for the sol-gel mechanism.[19]

There are many studies in the literature in which strontium titanate is produced by sol-gel besides solid-state synthesis and hydrothermal synthesis. Generally, raw materials such as $TiO(NO_3)_2$, $TiCl_4$, $Sr(NO_3)_2$ are used as starting materials.

In a study, strontium titanate ceramics were prepared using the sol-gel method, and their electrical properties were compared with powders produced by solid-state synthesis. Obtained powders by the sol-gel method exhibited better capacitor-varistor properties than powders produced by solid-state synthesis. The authors explained this because of the smaller particle size of the obtained powders via sol-gel.[43]

Table 2.2. Synthesis of strontium titanate ceramic powders by the sol-gel method in the literature.

Ingredients	**Conditions**	**Produced material(s)**	**Notes**	**Ref.**
$Ti(C_4H_9O)_4$, CH_3COOH and $Sr(NO_3)_2$	700-900°C for 2 h	$SrTiO_3$, Sr_2TiO_4, $SrCO_3$ and TiO_2		43
$C_{12}H_{28}O_4Ti$, CH_3COOH, C_2H_5OH and $Sr(CH_3COO)_2$	700°C for 2 h	$SrTiO_3$		44
$C_{12}H_{28}O_4Ti$, $C_2H_6O_2$, $C_6H_8O_7.H_2O$ and $Sr(NO_3)_2$	180°C for 10 h	$SrTiO_3$		45
$Ti(C_4H_9O)_4$, $Sr(NO_3)_2$, CH_3COOH and $C_2H_6O_2$	600-800°C for 4 h	$SrTiO_3$	Molar ratio of Sr/Ti:1	46
$C_{12}H_{28}O_4Ti$, CH_3COOH and SrO	900°C for 1 h	$SrTiO_3$	Molar ratio of Sr/Ti:1	47

2.3.3. Hydrothermal Synthesis

Strontium titanate ceramic powders are widely produced by hydrothermal synthesis. The hydrothermal method has attracted the attention of scientists since the 1900s. First, British scientist Sir Roderick Murchison used the term hydrothermal based on the movement of water with high temperature and pressure in the earth's crust, which creates different rocks and minerals.[48, 49] Understanding the formation mechanism of rocks under high temperature and pressure conditions has enabled the hydrothermal method to be simulated and developed in the laboratory.[50] The first successful synthesis by this method is mineral extraction. With the developing technology, hydrothermal synthesis has become a production method used interdisciplinary and combined with different methods. For instance, hydrothermal reaction sintering, hydrothermal hot pressing, hydrothermal extraction, hydrothermal oxidation, etc..[49]

Water is a significant part of the hydrothermal system. General requirements for the hydrothermal method; temperature ($25^{o}C < T < 1000^{o}C$), and pressure ($0.1\ MPa < P < 500\ MPa$). However, these given conditions change according to the limits of the autoclave used. The pressure and temperature generated in the system are affected by the filling rate of the autoclave.[48, 50, 51]

Hydrothermal method equipment types have developed in parallel with the development of technology. However, most of the first hydrothermal studies were carried out on gun barrels, which are the only closed chamber that can be used under the time conditions. Gun barrels provided the pressure required for hydrothermal conditions. The first autoclaves were similar in structure, as the gun barrels were sealed with welding or screws.[53]

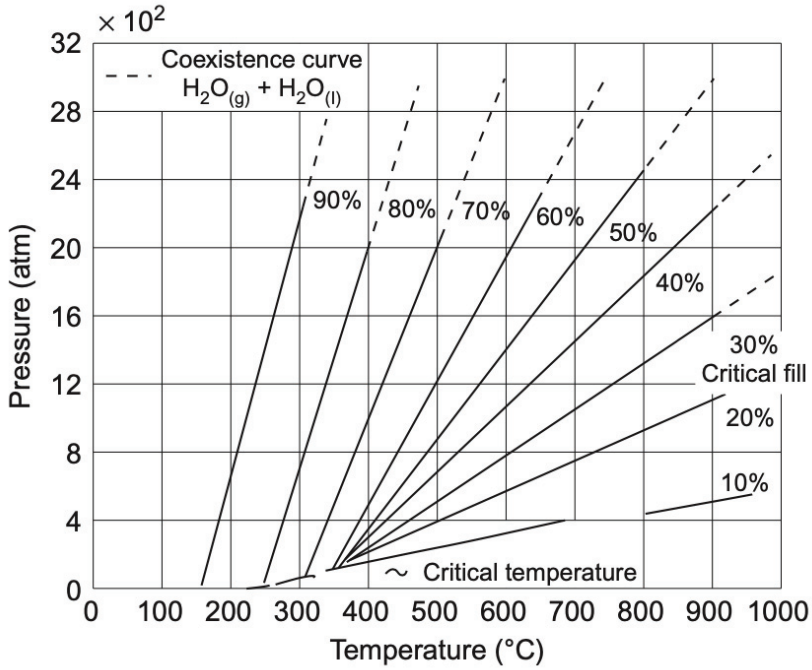

Figure 2.7. Pressure-temperature diagram for hydrothermal systems (Source: Kennedy, 1950).[52]

With the hydrothermal method, an insoluble solid phase is formed in the aqueous environment with the help of high pressure.[54] Hydrothermal synthesis is a process performed at a lower temperature compared to a solid-state reaction.[55, 56] With hydrothermal synthesis, pure ceramic powders can be produced in one step at relatively low temperatures, without the need for the calcination step at high temperatures.[6, 57] Control of synthesis conditions such as reaction temperature, pressure, time, filling rate, and pH allows the grain size and morphology to be controlled. The hydrothermal method enables powder synthesis at lower temperatures, low agglomeration, homogeneous particle distribution, and high purity product production.[40]

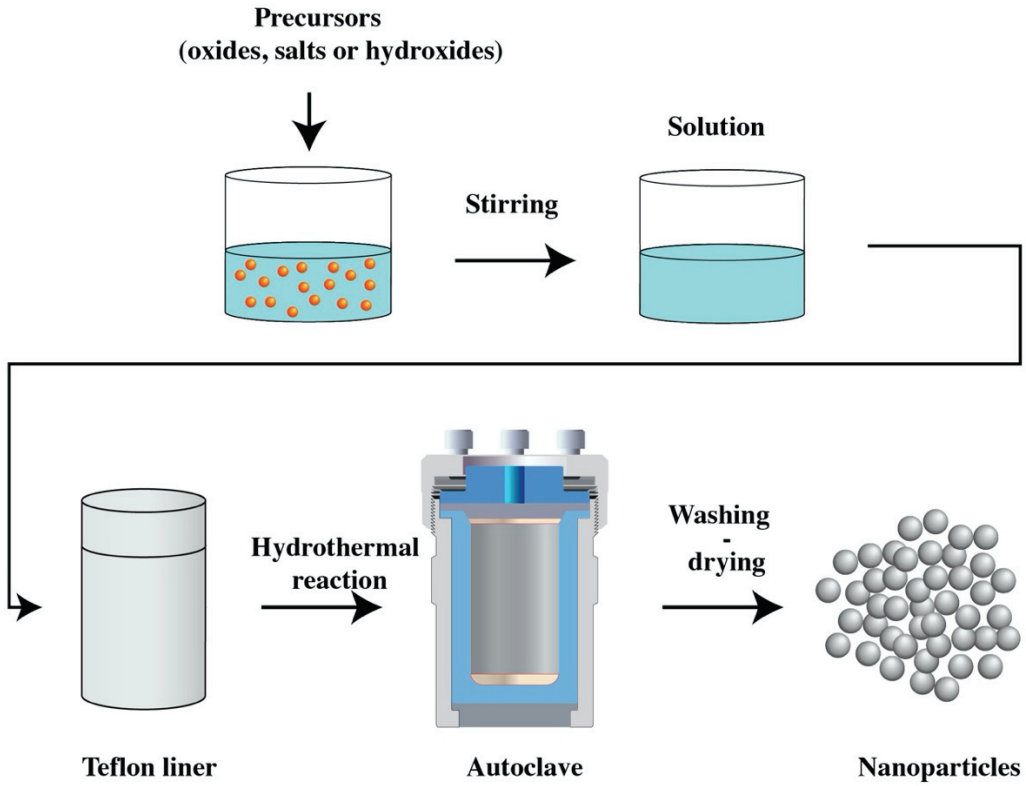

Figure 2.8. Schematic illustration for the hydrothermal synthesis.

Generally, raw materials such as $SrCl_4$, $SrCl_2.6H_2O$, $Sr(OH)_2.8H_2O$, $Sr(NO_3)_3$ [58-62] are used as strontium sources, while raw materials such as TiO_2, $Ti(OC_4H_9)_4$, $TiCl_4$, TiB_2 [58, 60, 63-65] are used as titanium sources. Among the important parameters affecting the production process of strontium titanate are the molar ratio of Sr/Ti, pH value of the solution, temperature, time, mineralizer, and filling ratio. In addition, these parameters greatly affect the properties of the final product.

There are many scientific studies using chlorides as a source of strontium. In the study, $SrCl_2.6H_2O$ and $TiO_2.nH_2O$ gel were used as starting materials, and KOH was added as a mineralizer to provide the appropriate pH value for the reaction. The prepared solution was subject to hydrothermal conditions at different times between 20 - 60°C. As a result, it was observed that the particle size of the final product, strontium titanate powders, was affected by the crystallinity of the gel. The particle size of the final product was controlled by the change of the crystallinity of the gel, and nanoparticles were produced under hydrothermal conditions.[58]

In another study, $SrTiO_3$ nanopowders were produced using $SrCl_2.6H_2O$ and $C_{12}H_{28}TiO_4$ at 140°C for 4 to 160 minutes with the microwave hydrothermal synthesis method. At the end of the reaction, with a molar ratio of Sr/Ti is 1, the strontium carbonate phase also presented in small amounts in addition to strontium titanate. It had been observed that the powders had a high rate of photoluminescence emission. At the end of the study, it was shown that the strontium titanate phase was relatively unaffected by the reaction time by looking at the XRD and Raman data.[66]

In another study, besides TiO_2 and $Sr(OH)_2.8H_2O$, NaOH was added to the solution as a mineralizer. The reaction was carried out under hydrothermal conditions with a Sr / Ti molar ratio of 1 and a strontium concentration of 0.2 mol/L. The temperature was kept constant at 200°C, and the time parameter varied between 15 minutes and 48 h. At the end of the reaction, significantly strontium titanate formation was observed in 15 minutes. However, even after 48 h, unreacted TiO_2 still remained. This is because, according to Kalyani et al., The reaction rate slows down as the reaction progresses. Besides the $SrTiO_3$ and TiO_2 phases, the $SrCO_3$ phase was also observed. Consequently, the contact of the starting materials with air, the reaction of CO_2 with $Sr(OH)_2$, which is a strong alkali, results in the undesired $SrCO_3$ phase.[12]

In another study, strontium titanate nano cubes were synthesized under alkaline conditions by hydrothermal method using TiO_2, $Sr(OH)_2.8H_2O$, and NaOH as starting materials, at different NaOH concentrations, temperatures, and times [64]. Previous studies have shown that Sr/Ti > 1 and high pH are required to synthesize high purity $SrTiO_3$ in the Sr-Ti system.[67] Similar to the previously mentioned studies, there were small amounts of $SrCO_3$ phase besides $SrTiO_3$ crystals. Since the pH value required for the precipitation of $SrCO_3$ is lower than the pH value required for $SrTiO_3$, $SrCO_3$ formation is common in hydrothermal systems.[68] At the end of the study, it was observed that the increase in NaOH concentration caused the particles to become spherical.[64]

Table 2.3. Synthesis of strontium titanate powders by the hydrothermal method in scientific studies.

Ingredients	Conditions	Produced material(s)	Notes	Ref.
$TiCl_4$ and $SrCl_2.8H_2O$ KOH/4 M	20-60°C for 0.6-2 h	$SrTiO_3$	N/A	58
TiO_2 (P25) and $Sr(OH)_2.8H_2O$ KOH/3 M	60-90-120-150-180°C for 72 h	$SrTiO_3$, TiO_2 and $SrCO_3$	@60°C incomplete	59
$Ti(OC_4H_9)_4$, $C_3H_8O_2$, $C_5H_8O_2$ and $Sr(OH)_2.nH_2O$ (n=4.6) KOH/0.6-4 M	85-100°C for 10-20 h	$SrTiO_3$		69
$(C_4H_9O)_4Ti$ and $Sr(OH)_2.8H_2O$ NAOH/12 M	90°C for 20 h	$SrTiO_3$ nanowires		60
$C_{12}H_{28}TiO_4$ and $Sr(NO_3)_3$ NAOH/4 M	100°C for 5 h	$SrTiO_3$	80% filling ratio	70
TiO_2 (P25) and $Sr(OH)_2.8H_2O$ NAOH/1-3-5-10 M	100-130-150-180°C for 24-48-72-96 h	$SrTiO_3$ and $SrCO_3$	Molar ratio of Sr/Ti >1	64
TiO_2 gel powder and $Sr(OH)_2.8H_2O$	110°C for 4 h	$SrTiO_3$	Molar ratio of Sr/Ti :1	61

(Cont. on the next page.)

Table 2.3. Cont.

$Ti(OCH(CH_3)_2)_4$ and $Sr(CH_3CO_2)_2$ NH_4OH	120°C for 12 h	$SrTiO_3$	pH:11	71
$Ti(OC_4H_9)_4$, $C_3H_8O_2$, H_2O, $C_5H_8O_2$ and $Sr(OH)_2.nH_2O$ (n=4.6) KOH/1.2-6 M	140-160°C for 12-24 h	$SrTiO_3$		69
$TiOSO_4.yH_2SO_4.yH_2O$ and $SrCl_2.2H_2O$ KOH/6 M	140°C for 0-8 h	$SrTiO_3$ and $SrCO_3$	Molar ratio of Sr/Ti :1	72
$TiOSO_4+xH_2O+H_2SO_4$ and $SrCl_2.2H_2O$ KOH	140°C for 10-160 min	$SrTiO_3$		73
$Ti(OC_4H_9)_4$ and $Sr(NO_3)_3$ NaOH	140°C for 24 h	$SrTiO_3$		74
TiO_2 gel and $Sr(OH)_2$ i-proponal	100-150°C for 2 h	$SrTiO_3$		75
$(CH_3CH(O^-)CO_2NH_4)_2Ti(OH)_2$ and $Sr(OH)_2.8H_2O$ NaOH/5 M	150°C for 72-96-120 h	$SrTiO_3$ and $SrCO_3$	Molar ratio of Sr/Ti:1 90% yield	62

(Cont. on the next page.)

Table 2.3. Cont.

TiO_2 (P25) and $Sr(OH)_2.8H_2O$ KOH/3.5 mmol	150°C for 72 h	$SrTiO_3$	pH=13	63
TiO_2 (P25) and $Sr(OH)_2.8H_2O$ KOH/50 M	150°C for 1-120 h	$SrTiO_3$	Molar ratio of Sr/Ti:10	76
TiO_2 and $Sr(OH)_2.8H_2O$	160°C for 40 h	$SrTiO_3$	Molar ratio of Sr/Ti:1	65
TiO_2 (P25) and $SrCl_2$ NaOH/1 M	160-240°C for 1-24 h	$SrTiO_3$ and TiO_2	When temperature increases $SrTiO_3$ spheres is larger.	77
TiO_2 and $Sr(OH)_2$ NH_3	170°C for 72 h	$SrTiO_3$	pH=13	78
$Ti(OBu)_4$ and $Sr(NO_3)_2$ NaOH/5 M	180°C for 24 h	$SrTiO_3$		79
$Ti(OC_4H_9)_4$, $Sr(Ac)_2$ and $C_8H_{16}O_2$	180°C	$SrTiO_3$		80

(Cont. on the next page.)

Table 2.3. Cont.

TiO_2 nanotubes and $Sr(OH)_2.8H_2O$	180°C for 1-3 h	$SrTiO_3$		81
TiO_2 and $Sr(OH)_2.8H_2O$	180°C for 12 h	$SrTiO_3$		82
TiO_2 and $SrCl_2.6H_2O$ NaOH/2 g	180°C for 6 h	$SrTiO_3$		83
TiO_2 and $SrCl_2.6H_2O$ NaOH/1 M	180°C for 6 h	$SrTiO_3$		84
TiO_2 and $Sr(OH)_2$ NaOH/5 M	180°C for 1 h	$SrTiO_3$	Molar ratio of Sr/Ti:1.0:0.98	85
TiB_2 and $Sr(NO_3)_2$ NaOH/3 M	200°C for 24-72 h	$SrTiO_3$	Molar ratio of Sr/Ti:1	86
TiO_2 and $Sr(OH)_2.8H_2O$ NaOH/5 M	200°C for 15 min-48 h	$SrTiO_3$, TiO_2 and $SrCO_3$	Molar ratio of Sr/Ti:1 Sr conc. 0.2 mol/L	12
TiO_2 and $Sr(CH_3CO_2)_2$ KOH/10 M	220°C for 24 h	$SrTiO_3$		87

(Cont. on the next page.)

Table 2.3. Cont.

TiO_2 and $Sr(OH)_2.8H_2O$ NaOH/50 M	220°C for 20-40-60 h	$SrTiO_3$	Molar ratio of Sr/Ti:1 and 2	[88]
$C_{12}H_{28}TiO_4$, $Sr(OH)_2.8H_2O$ and CH_3COOH NaOH/3 M	240°C for 12 h	$SrTiO_3$ and Sodium acetate hydrate	Molar ratio of Sr/Ti:1 mixing temperature: 95°C, pH=13	[89]
$C_4H_9O)_4Ti$ and $Sr(Ac)_2$ $C_3H_8O_3$	240°C	$SrTiO_3$	Molar ratio of Sr/Ti:1	[80]
$TiCl_4$ and $SrSO_4$ KOH/5 M	150-250°C and 0.08-96 h	$SrTiO_3$		[90]

2.4. Sintering of Strontium Titanate Ceramics

A sintering step is required to produce ceramic products after the production of ceramic powders. Ceramic powders produced by solid-state and hydrothermal methods are transformed into ceramic products by densifying with different sintering techniques.

2.4.1. Conventional Sintering

The process that allows powder components to become denser by reducing their pores and making them monolith is called sintering. For sintering to occur, a thermodynamic decrease in the free energy must occur between the two particles.[1]

Conventional sintering is generally examined in three groups. The green body is densified in solid-state sintering at temperatures that do not form a liquid phase. The pores are reduced, and the particles begin to join each other thanks to the atomic diffusion. In the liquid phase sintering, the solid mixture contains a certain amount of liquid by volume at sintering temperature. In liquid phase sintering, it is assumed that three stages follow each other: rearrangement, solution-precipitation, and removal of porosity. The first stage of liquid phase sintering is the redistribution of liquid and rearrangement of particles to achieve ideal densification. In the next stage, solution-precipitation, solids dissolve in areas with high chemical potential and precipitate in areas with low chemical potential. In the last stage, the reduction of the pores ensures densification. The liquid volume in viscous sintering, the third of conventional sintering, is about 25 to 30. It is widely used in the manufacture of ceramics. It is believed that in such a sintering process, the pores are filled with the support of viscous flow.[1]

In addition to conventional non-pressure sintering methods, there are also pressure-assisted methods such as the HIP. However, pressure-assisted methods are not economical compared to non-pressure methods. The pressure applied in these methods helps to densify. It is challenging to produce nanomaterials because of the high temperatures in traditional sintering methods. New methods such as spark plasma sintering have been developed to eliminate these problems.[1]

After the production of ceramic powders, a sintering step is required to produce ceramic products. Different sintering techniques are used to densify ceramic powders produced by methods such as solid-state and hydrothermal.

In traditional sintering methods, the sintering temperature is usually fired above 1000°C.[17, 27, 31] In a study, strontium titanate ceramic powders produced by solid-state synthesis were then sintered at 1440°C. After sintering, the relative density values of the samples were more than 97%.[30]

Table 2.4. Sintering conditions of strontium titanate ceramic powders in scientific studies.

Ingredients	Methodology	Conditions	Produced material(s)	Notes	Ref.
TiO_2 and $SrCO_3$	Solid-state synthesis	Sintering: 1000-1100-1200-1300-1400°C for 10 h	$SrTiO_3$ $SrCO_3$	Incomplete formation of $SrTiO_3$ in samples sintered lower than 1200°C.	29
TiO_2 and $SrCO_3$	Solid-state synthesis	Sintering: 1400°C for 10 h	$SrTiO_3$		27
TiO_2 and $SrCO_3$	Solid-state synthesis	Sintering: 1440°C for 2 h	$SrTiO_3$	Relative density of all sintered samples is more than 97% Sr/Ti>1 small grain size Sr/Ti<1 larger grain size	30
TiO_2 and $SrCO_3$	Solid-state synthesis	Sintering: 1200°C for 1 h	$SrTiO_3$		17
TiO_2 and $SrCO_3$	Solid-state synthesis	Sintering: 1500°C for 1 h and 1450°C for 9 h	$SrTiO_3$		31
TiO_2 and $SrCO_3$	Solid-state synthesis	Sintering: 1400-1480-1600°C for 4-20 h	$SrTiO_3$		35

(Cont. on the next page.)

Table 2.4. Cont.

TiO_2 and $SrCO_3$	Solid-state synthesis	Sintering: 1100°C for 48 h	$SrTiO_3$		25
TiO_2 and $SrCO_3$	Solid-state synthesis	Sintering: 1250°C for 20 h	$SrTiO_3$		36
TiO_2 and $SrCO_3$	Solid-state synthesis	Sintering: 1100°C for 24 h	$SrTiO_3$		26
TiO_2 and $SrCO_3$	Solid-state synthesis	Sintering: 1100°C for 24 h	$SrTiO_3$		37

Recently, new methods have been developed that provide densification at lower temperatures than conventional sintering methods. With the new methods developed in recent years, it has become possible to produce monolithic ceramics in one step without the need for two steps, such as powder production stage and sintering. These methods are referred to as low-temperature densification methods.

2.4.2. Low Temperature Densification Methods

Sintering is a process that has existed for thousands of years. Many processes, such as lithification, are an example of sintering that occurs spontaneously in nature. Lithification is when free particles are compressed to form rocks by densifying with a decrease in porosity. Very high pressures are required for this formation. Whereas very high pressures can occur in nature, it is not possible to reach these pressures in the industry. These formations, which spread over very long periods of time in nature, must occur in much shorter periods in production.[1]

Recently, with the idea of reducing carbon footprint and protecting nature, scientists have taken inspiration from nature and turned to research new methods that are more environmentally friendly and economical. In this direction, new technologies have been developed that enable the production of monolithic ceramics in one step by combining the powder synthesis and sintering step at lower temperatures. In the low-temperature densification methods, densification takes place at low temperatures, unlike traditional sintering methods[1]

These pressure-assisted methods at relatively low temperatures are hydrothermal reaction sintering, hydrothermal hot pressing, cold sintering, and reactive hydrothermal liquid-phase densification.[1]

2.4.2.1. Hydrothermal Reaction Sintering (HRS)

Metal powders are generally used in the hydrothermal reaction sintering method, which enables ceramic materials with high relative densities to be obtained. The reaction between pure metal powder (Me) and water (H_2O) requires a temperature varying between 500^{o}C and 1000^{o}C and a certain pressure. The metal oxide is obtained as the reaction product, and hydrogen gas is released from the reaction. As the gas leaves the system, it increases the reaction efficiency by contributing to the increase of the pressure of the system.[1]

Figure 2.9 shows monolithic Cr_2O_3 production by the hydrothermal reaction sintering method. Cr metal powders and water reacted in a capsule made of platinum or gold. The capsule is placed in a closed system. As a result of the reaction at 1000^{o}C temperature and 98 MPa pressure, Cr_2O_3 and H_2 gas were obtained. The relative density of the Cr_2O_3 ceramic has reached 99.2 %.[1]

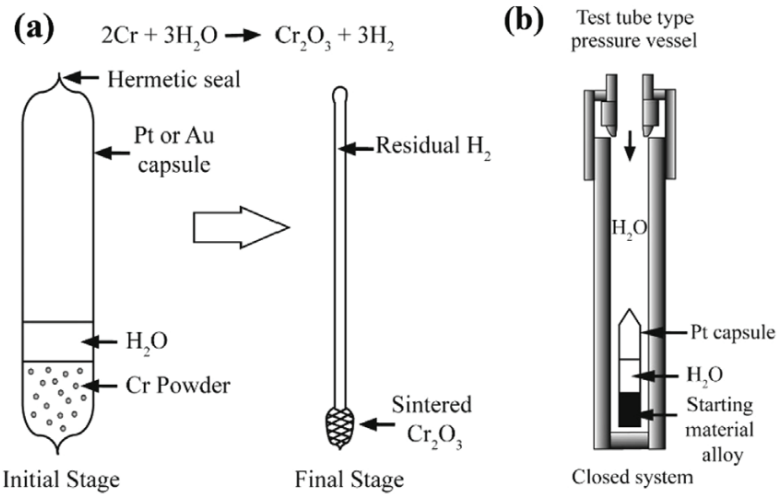

Figure 2.9. (a) Representation of Cr_2O_3 production with HRS method, and (b) Equipment used for HRS (Source: Sõmiya, 2012).[91]

2.4.2.2. Hydrothermal Hot Pressing (HHP)

Hydrothermal hot pressing is used for sintering inorganic components at lower temperatures than the hydrothermal reaction sintering method. In the hydrothermal hot pressing method, the temperature is generally below 500°C, and the reaction takes place under hydrothermal conditions. It takes place at low temperatures, such as lithification, which is one of the sintering processes in nature, has made it known as artificial lithification.[1]

In the HHP process, it is essential to compact the powder and remove water from the system. If the sample is not compressed enough to remove water from the sample, the water remains in the sample and causes the formation of pores. Pore formation causes low relative density.[1]

2.4.2.3. Cold Sintering (CS)

In the cold sintering method, ceramic powders are densified under medium and high pressures and at relatively low temperatures (< 350°C) due to the liquid addition to the system[1]

The system consists of a uniaxial press and resistance jacket. During the compression provided by the press, the mold placed inside the resistance jacket is heated. During the process, the added fluid moves away from the system, and the sample densifies.[1]

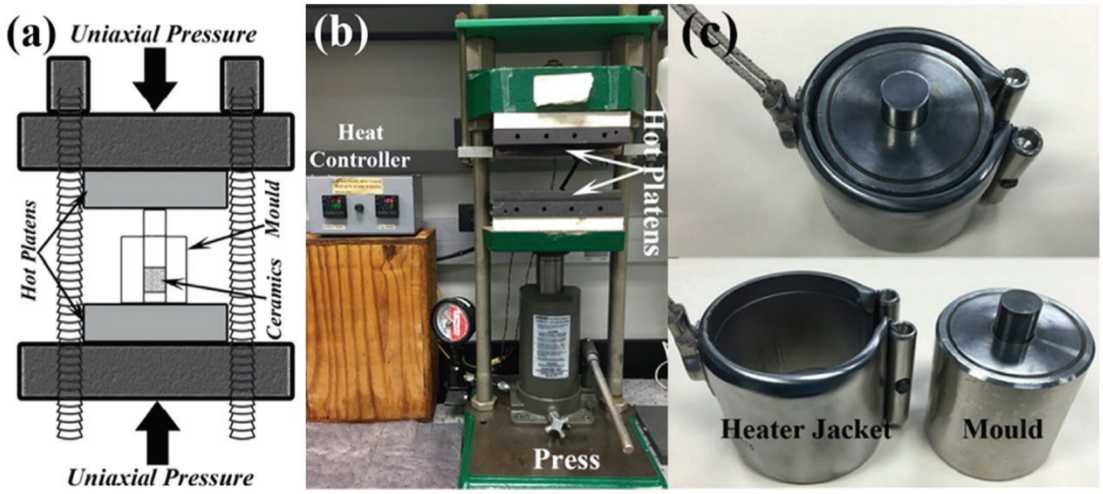

Figure 2.10. (a) Schematic of an uniaxial press, (b) Equipment used in cold sintering experiments, and (c,d) Mold parts used in cold sintering (Source: Guo, 2016).[92]

2.4.2.4. Reactive Hydrothermal Liquid-Phase Densification (rHLPD)

Recently, developing technology and the idea of protecting nature have led scientists to research new methods that are more environmentally friendly and

economical. For this purpose, new technologies have been developed that enable the production of monolithic ceramics in one step by combining the powder synthesis and sintering step at lower temperatures. In the low-temperature densification methods, densification takes place at low temperatures, unlike traditional sintering methods. One of the new technologies developed is the reactive hydrothermal liquid-phase densification method, which provides densification at low temperatures. rHLPD is a method used to produce monolithic ceramic materials at low temperatures. This method can be used to densify composite systems such as $BaTiO_3[TiO_2]$, $SrTiO_3[TiO_2]$, $Ca(PO_4)F_2[CaF_2]$.[93]

The reactive hydrothermal liquid-phase densification method is basically based on four principles: hydrothermal reaction, infiltration, reactive crystallization, and liquid phase sintering.[1, 93]

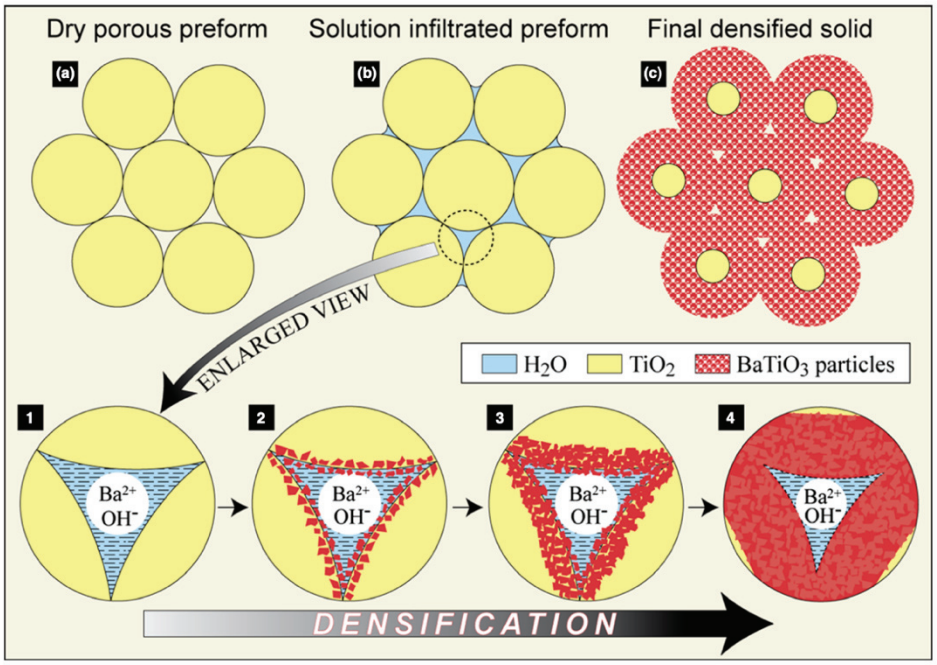

Figure 2.11. Schematic of rHLPD process sequences (Source: Vakifahmetoglu, 2016).[93]

The sequence of the process of rHLPD is given in Figure 2.11. In the first step, a porous matrix is formed using conventional methods. It is possible to prepare the green body in various sizes and shapes by shaping methods such as extrusion, dry pressing, dip

coating. For example, in the $BaTiO_3[TiO_2]$ system, the matrix is TiO_2. The TiO_2 green body can be prepared by any desired shaping method.[93]

The second stage is the infiltration step. A liquid is prepared of soluble reactive cations or anions which the porous matrix will react. Then, an unstable hydrothermal reaction, which is thermodynamically preferred, is initiated to react to the matrix and liquid. During the reaction, reaction products are formed that fill the pore space of the green compact. As mentioned before, in the $BaTiO_3[TiO_2]$ ceramic composite system, the matrix is TiO_2 by brackets, and the product formed is $BaTiO_3$. More than one infiltration occurs in a system such as $Sr(PO_4)(OH)_2[SrTiO_3]$. First, TiO_2 is used as a matrix, and $SrTiO_3$ is formed. Subsequently, $SrTiO_3$ forms the final product, strontium apatite, as a porous matrix in the second infiltration. Thus, ceramic products in a wide variety of compositions can be obtained via the rHLPD method.[93]

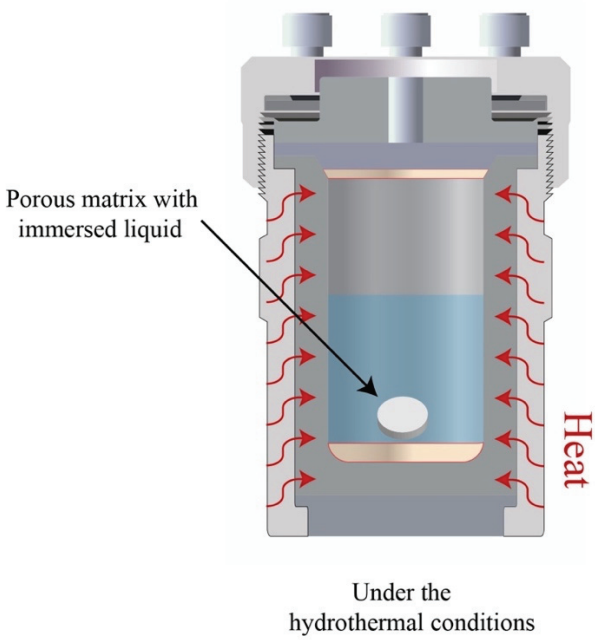

Figure 2.12. Experimental process for rHLPD method.

Thanks to the hydrothermal reaction kinetics in the rHLPD system, product formation occurs at temperatures between approximately 100°C-300°C. An essential parameter in rHLPD is choosing a product with a larger molar volume than the molar volume of the matrix. In this way, the reaction proceeds to fill the pores of the matrix.

Crystal formation in the pores of the matrix increases the molar volume. The crystals thus formed can nucleate homogeneously in the pores and grow epitaxially from other crystals.[93]

In the rHLPD method, there is no volumetric size change since there is no transport process. Thus, ceramic materials can be densified without any change in size with the rHLPD method. Due to high temperature phase transformations that usually occur in high temperature sintering methods, mechanical defects can be eliminated with rHLPD.[93]

2.5. Properties and Applications of Strontium Titanate Ceramics ($SrTiO_3$)

Strontium titanate has various uses in the electroceramic industry, gas sensors, and optical applications because of its wide variety of properties.[94] $SrTiO_3$ is used as a substrate in epitaxial growth applications due to its high temperature resistance. $SrTiO_3$ has a high dielectric constant of about 300 at room temperature.[13] Strontium titanate ceramics has a pure state band gap of 3.2 eV, so it is only used as a photocatalyst in UV wavelength for water separation processes ($\lambda < 387.5$ nm).[13]

Table 2.5. Properties and applications of strontium titanate ceramics.[13, 83, 96-98]

Properties of strontium titanate ceramics	Applications of strontium titanate ceramics
High dielectric constant (~300)	Oxygen gas sensors
Nonlinear refractive index (at 1064 μm 48.5 x10^{-20} m^2 W^{-1})	Optical memories

(Cont. on the next page.)

Table 2.5. Cont.

High thermal and chemical stability	Electrooptic modulators
Large dielectric tunability	Thin-film capacitors
Low microwave losses	Water splitting process

$SrTiO_3$ has been the potential material for tunable microwave devices operating at extremely low temperatures, thanks to their low microwave losses and high dielectric constant.[23, 95] In addition, strontium titanate ceramics are also used in high voltage capacitors. Since the melting point of strontium titanate is around 2080°C, it has become a material that can be used for high temperature applications.[13]

CHAPTER 3

EXPERIMENTAL PROCEDURE

3.1. The Raw Materials

Strontium titanate ceramics are mainly manufactured using $Sr(OH)_2.8H_2O$ (99 % pure, CAS 1311-10-0 Alfa Aesar), TiO_2 (99.8 % anatase, molecular weight: 79.87 g/mol, density: 3.9 g/mL, CAS 1317-70-0 Sigma Aldrich Chemistry), NaOH (molecular weight: 40.00 g/mol, CAS 1310-73-2 Sigma Aldrich Chemistry) and PVA (CAS 9002-89-5 Sigma Aldrich Chemistry). Deionized water (Ultrapure Type-I, 18.2 MΩ.cm at 25.2^oC) was supplied from the Millipore Direct-Q® 8 UV water treatment system.

3.2. Equipments

Retsch planetary ball mill PM100 was used to prepare the TiO_2 green body. In the second stage, Parr industrial acid digestion vessel 4748A model static autoclave was used. The working temperature and pressure of the autoclave are maximum 250^oC and 13 (131) MPa.

3.3. Experimental Procedure of rHLPD

For the reaction to occur in the rHLPD process, there must be a conversion from the green body to the densified pellet. This conversion occurs with an increase in molar

volume. The total reaction for the $Sr(OH)_2$–TiO_2–H_2O ternary equilibrium is written in Eq. II:

$$Sr(OH)_2 + TiO_{2(s)} \rightarrow SrTiO_{3(s)} + H_2O \qquad (II)$$

$Sr(OH)_2$ immersed liquid, TiO_2 matrix, $SrTiO_3$ and H_2O are the final product. Supposing the reaction will be completed to 100 %, if TiO_2 is completely converted to $SrTiO_3$, 75.12 % molar volume expansion is expected ($V^{m}_{TiO2} = 20.2\ cm^3/$ mole $\rho^{anatase}_{TiO2} = 3.895\ g/cm^3$ and $V^{m}_{SrTiO3} = 35.90\ cm^3/mole\ \rho_{SrTiO3} = 5.11\ g/cm^3$).

Theoretical density values were figured out using the rule of mixtures (ROM, with Eq. (III)), using phase ingredients volume fraction from mole conversion calculation).

$$\rho_{th} = \left(V_{SrTiO_3}\rho_{SrTiO_3}\right) + \left(V_{TiO_2}\rho_{TiO_2}\right) + \left(V_{SrCO_3}\rho_{SrCO_3}\right) \qquad (III)$$

Final relative density (% theoretical density), evidence of after-reaction density, can be shown as $\%\rho_{th} = 100(\frac{\rho_b}{\rho_{th}})$. The porosity (P) in the pellet after the reaction is denoted by $P = 100 - \%\rho_{th}$).

3.3.1. Green Body Preparation

The porous green body was obtained by dry pressing. To prepare a porous matrix, a 10 % by weight PVA solution was first prepared. Then 1 gram of polyvinyl alcohol (PVA) solution, 12 ml of DI water, and 3 g of TiO_2 powder were ground at 250 rpm for 24 h with zirconia balls in the ball mill (Retsch PM-100, Germany). After the grinding stage, the sludge obtained was dried in an oven at 80°C. After the drying process, the agglomerated powder was ground and sieved in a 45 mesh. Then, the obtained powder

(0.2 g) was dry pressed into 10x10 mm diameter and 1.2 mm thick pellets at 40 MPa in a Specac press. The pellets containing PVA were subjected to the binder-burnout process at 400°C for 5 h. The binder burnout stage is necessary to remove organic components from the green body and for the hydrothermal reaction to take place. Organic components can be removed from the body with the binder burnout. [93]

3.3.2. Hydrothermal Reaction

Strontium hydroxide octahydrate ($Sr(OH)_2.8H_2O$), and DI water were mixed in a magnetic stirrer, and then water was added so that the final volume is 70 %. Before the reaction, the prepared binderless TiO_2 pellets were weighed, and their diameter and thickness measurements were taken. Then the prepared solution was first used for pre-infiltration of the binderless porous matrix. Pre-filtration was necessary to prevent the binderless green body from being affected by capillary stresses during the hydrothermal reaction. For infiltration, a binder-free porous matrix was placed on Teflon, then 3 drops were dropped on both sides with the prepared hydroxide solution. It was left for a few minutes after the green bodies were infiltrated. After the binderless green body is infiltrated with the prepared solution, The TiO_2 green body and the hydroxide solution were poured into Teflon. Then the Teflon was placed into the autoclave, and finally, the hydrothermal reaction was performed with different temperature and time parameters. After the reaction was completed, the autoclave was opened, the pellet was taken from the solution, washed several times with DI water, and dried at 80°C for 1 day.

3.3.3. Reaction Parameters

During this thesis, while working on the production of strontium titanate with rHLPD, three different parameters such as temperature, time, and NaOH concentration were changed, and the effects of these parameters on strontium titanate ceramics were investigated. The amount of strontium hydroxide octahydrate, $Sr(OH)_2.8H_2O$, was used

0.3 M throughout the study. Firstly, experiments were done at temperatures ranging from 90°C to 200°C at 24 h (Table 3.1.).

Table 3.1. Reaction parameters of experiments carried out at different temperatures.

Sample code	Time (h)	Temperature (°C)	Filling ratio (%)
T1	24	90	70
T2	24	120	70
T3	24	140	70
T4	24	160	70
T5	24	180	70
T6	24	200	70

As the densification reached its highest value at 120°C and 140°C due to experiments performed at different temperatures, time and NaOH concentration experiments were carried out at these two temperatures. In the experiments done to see the time effect, the time was determined as 6, 24 and 72 h (Table 3.2.).

Table 3.2. Reaction parameters of experiments performed at different times.

Sample code	Time (h)	Temperature (°C)	Filling ratio (%)
R1	6	120	70

(Cont. on the next page.)

Table 3.2. Cont.

R2	24	120	70
R3	72	120	70
R4	6	140	70
R5	24	140	70
R6	72	140	70

The effect of additional NaOH concentration, which is another parameter, was investigated after the temperature and time experiments. Experiments were done at 120ºC and 140ºC at 24 h by adding three altered molarities of NaOH to the solution (Table 3.3).

Table 3.3. Reaction parameters of experiments performed with the addition of varied NaOH concentrations.

Sample code	**NaOH (M)**	**Time (h)**	**Temperature (ºC)**	**Filling ratio (%)**
N1	0.1	24	120	70
N2	0.5	24	120	70
N3	1	24	120	70
N4	0.1	24	140	70

(Cont. on the next page.)

Table 3.3.

N5	0.5	24	140	70
N6	1	24	140	70

3.4. Characterization Method

The fraction surface morphology of the monolithic samples was analyzed by Scanning Electron Microscopy (SEM; Quanta 250, FEI, Hillsboro, OR, USA). SEM analysis was performed by coating the surface of the pellets with approximately 10nm Au. After the monolithic strontium titanate ceramics were ground, X-ray diffraction measurements with CuK_{α} radiation were made with the Philips X'Pert Pro device. The scanning step was 0.005^{o}/second during the measurement, and phase analysis was performed between 10-90^{o}. Rietveld analysis was carried out using ReX software, starting from a two-phase sample model including the $SrTiO_3$ and TiO_2 reference crystal structures. Bulk densities of the samples were measured by the Archimedes liquid immersion method with ethanol. After the samples were ground and dried, they were mixed with potassium bromide, and pressed into pellets for FTIR analysis (PerkinElmer, UATR Two, Waltham, MA, USA). For Fourier Transform Infrared spectra, measurements were taken by performing 20 scans between 400 and 4000 cm^{-1} in transmission mode.

CHAPTER 4

RESULTS AND DISCUSSION

4.1. Microstructure and Phase Analysis of TiO_2 Green Body

The microstructure of the TiO_2 green body was analyzed before the reaction. SEM images and the XRD pattern of the porous matrix are given in Figure 4.1.

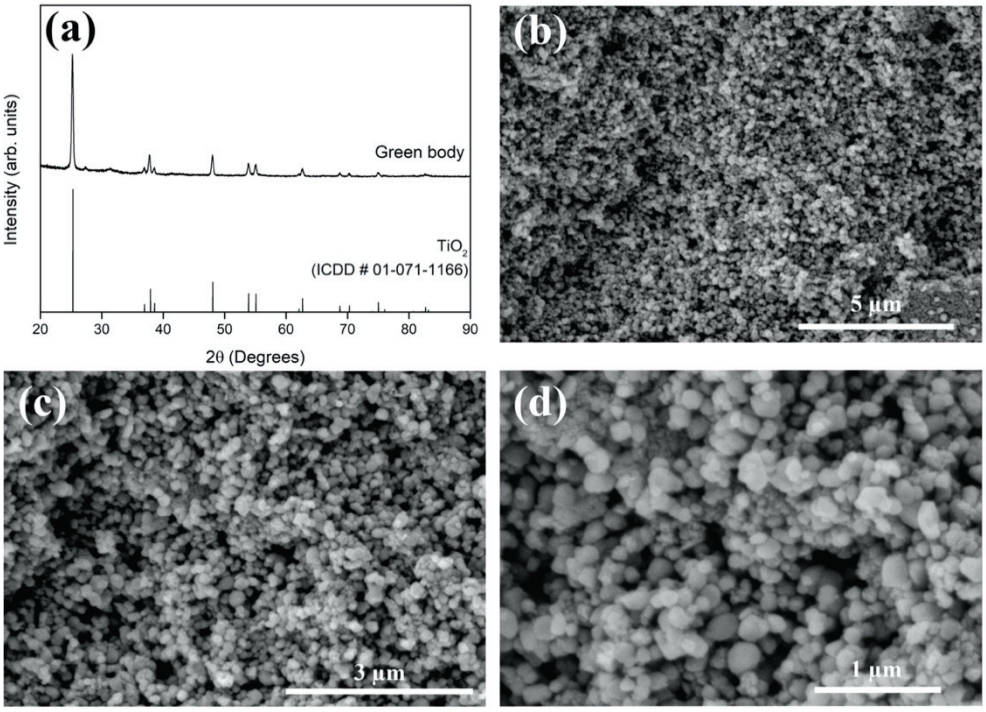

Figure 4.1. (a) XRD pattern of TiO_2 green body, and (b-d) Different magnification SEM images from fracture surface of TiO_2 green body. ICDD database for TiO_2 (ICDD # 01-071-1166 is also included in the figure.

The phase analysis result was consistent with the anatase phase (ICDD # 01-071-1166), as shown in Figure 4.1. The porous structure of the green body can be seen in SEM images at different magnifications. The relative densities of TiO_2 green bodies used in all studies varied between 51± 3.2%.

4.2. Mole Conversion Calculation

The mole conversion (%) values were calculated over the reaction that would occur if the reaction theoretically took place with a 100 % yield. To explain with an example calculation, if we calculate the mole conversion for the T1 sample when 0.19 g TiO_2 is used, the amount of $SrTiO_3$ to be obtained when the reaction is completed with 100 % yield should be 0.440 g (Equation IV). In reaction IV, the minus sign means consumed, plus means produced. Assuming that the $SrTiO_3$ pellet consists of SrO and TiO_2, the amount of SrO is found by subtracting the amount of TiO_2 used from the amount of $SrTiO_3$ that should be formed.

$$SrO + TiO_2 \rightarrow SrTiO_3 \qquad \text{(IV)}$$

$$\downarrow \qquad \downarrow$$

-0.0024 mol (0.19 g) +0.0024 mol

+0.440 g should have been.

The weight of the pellet formed after the reaction was 0.283 g. If the initial pellet weight is subtracted from the 0.283 g pellet weight, the amount of SrO (0.093 g: 0.0089 mol) in the formed pellet is found. Then a new equation is written, and calculations according to the limiting component of SrO are done as follows (Equation V).

$$SrO + TiO_2 \rightarrow SrTiO_3 \qquad \text{(V)}$$

$$\downarrow \quad \downarrow$$

0.0089 mol 0.0024 mol

0.0089 mol - 0.0089 mol + 0.0089 mol

0.0001 mol= 0.118 g TiO_2 remaining in the pellet) 0.00089 mol = 0.164 g (occurred $SrTiO_3$)

After finding the amount of $SrTiO_3$ obtained and the amount of $SrTiO_3$ that will occur when the reaction is carried out with 100% yield, the mole conversion value from Equation VI is calculated as approximately 37%.

$$\text{Mole conversion \%: } \frac{\text{occured } SrTiO_2\,(\text{mol})}{\text{should occur } SrTiO_2\,(\text{mol})} \qquad \text{(VI)}$$

4.3. Effect of Reaction Temperature

According to the mole conversion values calculated in the rHLPD experiments performed at different temperatures, the densification was at the lowest level at 90°C. Mole conversion values with standard deviation values are given in Table 4.1. In the experiments done at different temperatures, the mole conversion values increased from 90°C to 140°C and then decreased.

Table 4.1. Density and mole conversion values of green body and sintered body, (green body reacted different reaction temperatures for 24 h).

Sample code	**T (°C)**	**Green body bulk density (g/cm^3)**	**Green body relative density (%)**	**Sintered body bulk density by geometric (g/cm^3)**	**Sintered body bulk density by Archimedes (g/cm^3)**	**Mole conversion (%)**
T1	90	2.08 (±0.02)	52.80 (±0.70)	2.96 (±0.87)	2.92 (±0.07)	37.11 (±0.86)
T2	120	2.09 (±0.01)	53.57 (±0.38)	3.80 (±0.23)	3.67 (±0.03)	58.90 (±1.84)
T3	140	2.03 (±0.02)	52.11 (±0.82)	3.50 (±0.11)	3.53 (±0.01)	56.70 (±1.12)

(Cont. on the next page.)

Table 4.1. Cont.

T4	160	1.99 (±0.04)	50.49 (±1.83)	3.17 (±0.18)	3.22 (±0.04)	48.17 (±0.21)
T5	180	2.03 (±0.02)	52.18 (±0.53)	3.40 (±0.25)	3.27 (±0.10)	45.39 (± 3.78)
T6	200	1.98 (±0.03)	51.37 (±0.95)	3.18 (±0.33)	3.24 (±0.06)	45.75 (±2.12)

It was also understood from the theoretical density values that the decrease in the pores occurs due to the reaction. Theoretical density values of sintered bodies consisting of TiO_2 and $SrTiO_3$ calculated from the rule of mixtures (ROM) equation are given in Table 4.2. Moreover, densification was the best at 120°C and 140°C. Final relative density value expresses how dense the pellets are and what percentage of porosity they have. While the relative density value of the green body was 50 %, the final relative density value of the sintered sample reacted at 120°C reached 77.57 %.

Table 4.2. Density and porosity values of rHLPD samples reacted at different reaction temperatures for 24 h.

Sample code	**Sintered body bulk density by Archimedes (g/cm^3)**	**Sintered body theoretical density (via ROM) (g/cm^3)**	**Final relative density ($\%\rho_{th}$)**	**Porosity (P) (vol%)**
T1 (90°C-24 h)	2.92 (±0.07)	4.51 (±0.01)	64.54 (±1.54)	35.46 (±1.54)
T2 (120°C-24 h)	3.67 (±0.03)	4.75 (±0.02)	77.90 (±0.90)	22.10 (±0.90)

(Cont. on the next page.)

Table 4.2. Cont.

T3 (140°C-24 h)	3.53 (±0.01)	4.70 (±0.04)	73.27 (±2.60)	26.73 (±2.60)
T4 (160°C-24 h)	3.22 (±0.04)	4.35 (±0.40)	71.38 (±3.61)	28.61 (±3.61)
T5 (180°C-24 h)	3.27 (±0.10)	4.47 (±0.24)	71.73 (±2.00)	28.26 (±2.00)
T6 (200°C-24 h)	3.24 (±0.06)	4.43 (±0.32)	70.67 ±4.12)	29.33 (±4.12)

Figure 4.2 (a-f) shows SEM micrographs of fracture surfaces of samples reacted for 24 h at different temperatures. As seen in the SEM images, the sample reacted at 90°C and has a porous structure. In Figure 4(b), it is seen that the porous structure of the sample, which reacted at 120°C, is relatively reduced and densification is achieved. As the temperature started to rise from 120°C, the mole conversion values began to decrease. As seen in SEM micrographs, the samples have a porous structure.

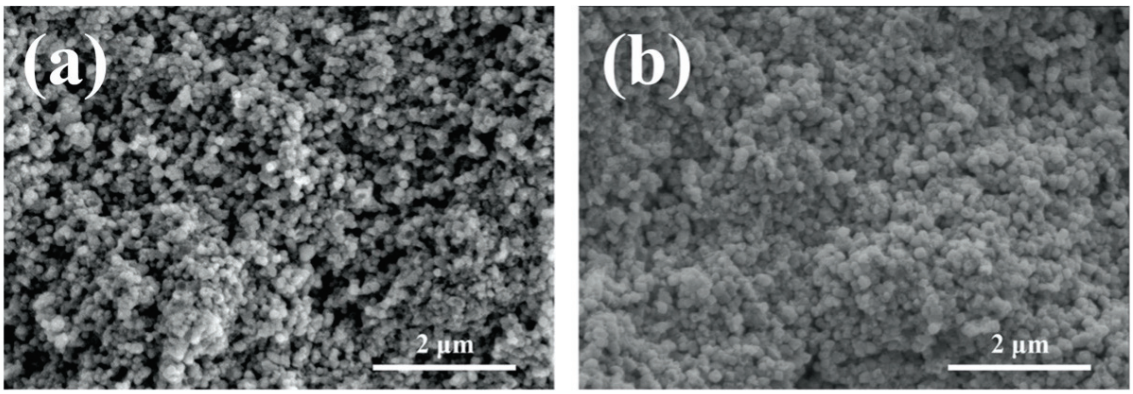

Figure 4.2.(Cont. on the next page)

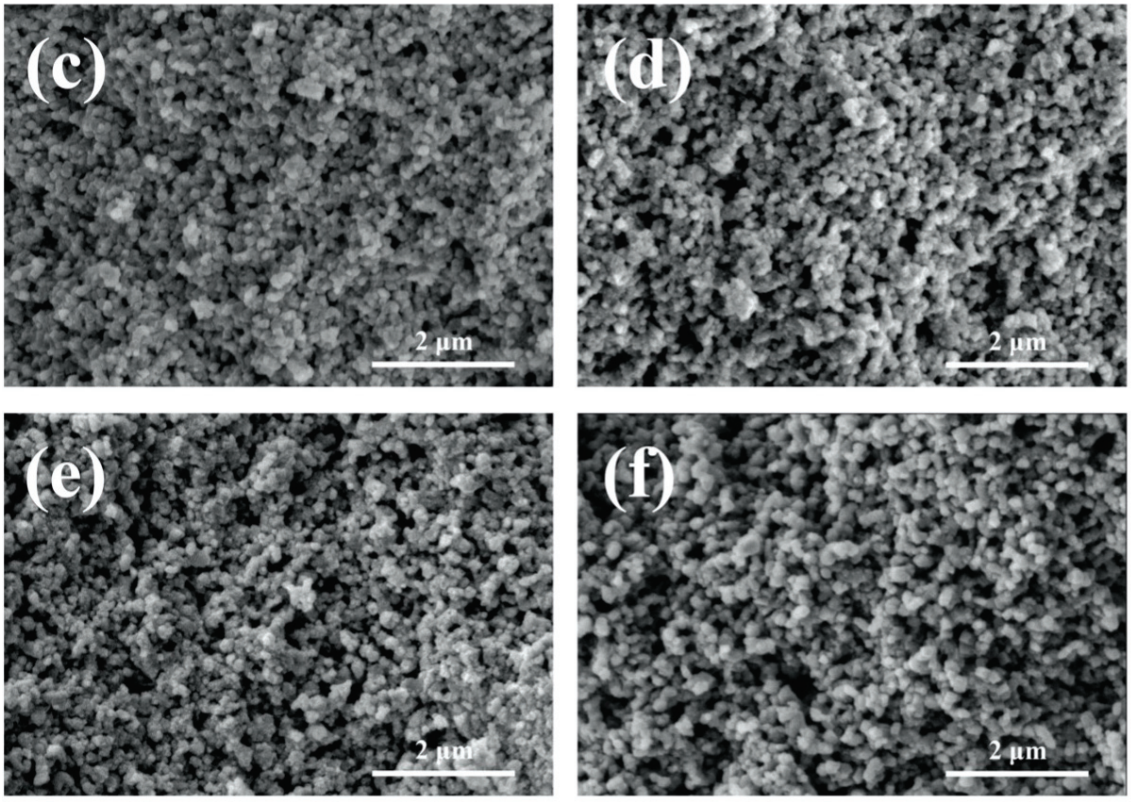

Figure 4.2. SEM images of the fracture surfaces of the pellets obtained at different temperatures while keeping reaction times for 24 h: (a) T1 (90°C), (b) T2 (120°C), (c) T3 (140°C), (d) T4 (160°C), (e) T5 (180°C), and (f) T6 (200°C).

XRD patterns of the experiments are given in Figure 4.3. According to the XRD analysis of the experimental set performed at different temperatures, ICDD No # 01-071-1166 TiO_2 remained in the structure in all samples. There were ICDD No # 01-073-0661 $SrTiO_3$ and ICDD No # 01-071-1166 TiO_2 in all experiments in the general structure.

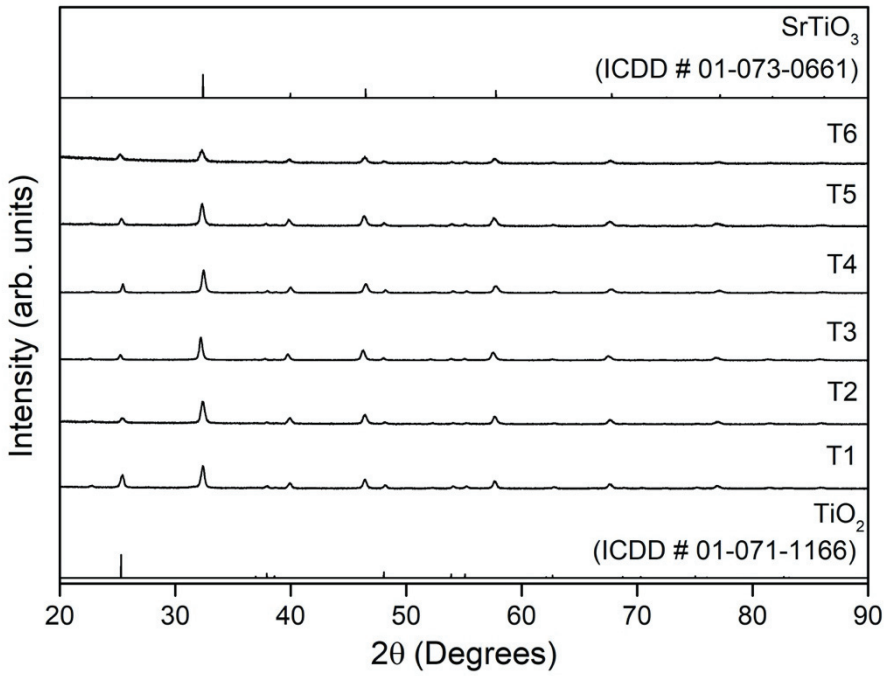

Figure 4.3. XRD patterns of obtained samples at different temperatures: (T1: 90°C/ T2: 120°C/ T3: 140°C/ T4: 160°C/ T5: 180°C/ T6: 200°C). ICDD database for TiO_2 (ICDD # 01-071-1166), and $SrTiO_3$ (ICDD # 01-073-0661) are also included in the figures.

The quantitative data of some experiments performed at different temperatures and the Rietveld fit of the sample at 120°C, which had the highest densification among temperature experiments, are given in Table 4.3 and Figure 4.4, respectively. The R_{wp} fitness values given in the table illustrate an excellent fit between the experimental data and the calculated model. The volume fraction values found in the mole conversion calculations and the data extracted from the Rietveld analysis matched each other. According to the quantitative results, the sample, which reacted for 24 h at 120°C, had 71.37 % $SrTiO_3$ phase by volume.

Table 4.3. Quantitative results of $SrTiO_3$ samples reacted by different conditions (T1: 90°C- 24 h / T2: 120°C- 24 h / T3: 140°C- 24 h)

Sample code	R_{wp}	TiO_2 phase (%vol.)	$SrTiO_3$ phase (%vol.)	Phase domain size (Å) (TiO_2)	Phase domain size ($SrTiO_3$)
T1	0.0879	54.80	45.20	267	263
T2	0.0712	28.63	71.37	356	332
T3	0.0831	30.04	69.96	360	276

The Rietveld refinement of the sample, which reacted at 120°C and 24 h reaction conditions, is given in Figure 4.4. Rietveld refinement showed that the sample had $SrTiO_3$ and TiO_2. It also supports that the $SrCO_3$ phase, which was not seen in previous XRD analyses, was not found in the structure.

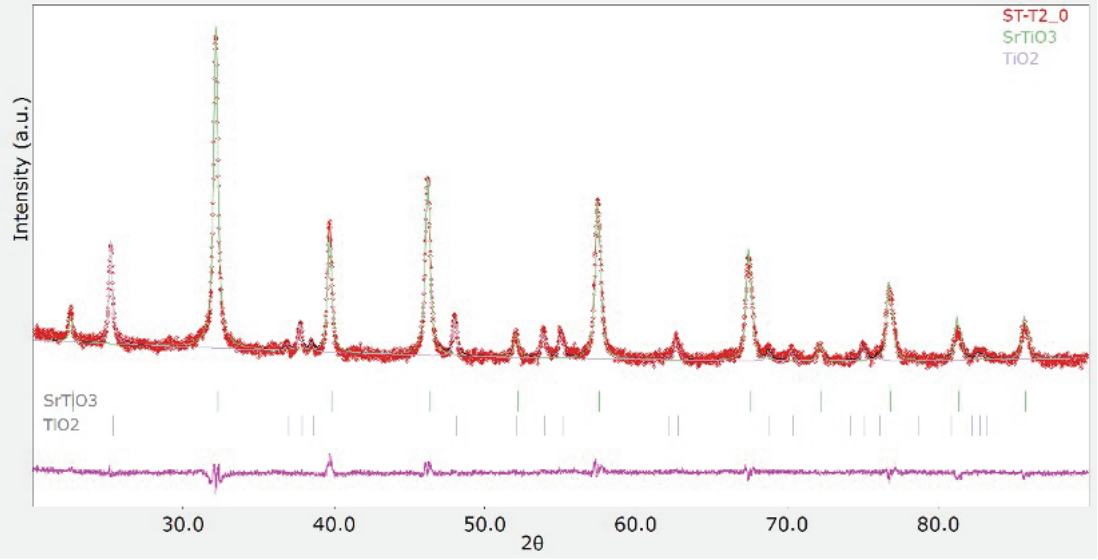

Figure 4.4. Rietveld fit of $SrTiO_3$ reacted at 120°C for 24 h (T2). Below the pattern, the peaks of the $SrTiO_3$ and TiO_2 phases are shown.

4.4. Effect of Reaction Time

In this experimental set, the temperature values were limited to 120°C and 140°C. In this experimental set, which was carried out with the temperature values with the highest mole conversion values in the temperature experiments, t=6/24/72 h was chosen. T=120°C and 140°C, t=24 h experiments were not repeated as they have been observed before.

Mole conversion values increased depending on the reaction time in experiments performed at different times. Table 4.4 shows that mole conversion values increased in direct proportion to the time. While the mole conversion was 40.80 % at 120°C, t:6 h, it was 68.87 % at t:72 h. A similar increase was observed in the experiments performed at 140°C. While the mole conversion was 55.82 % at 140°C t:6 h, it was 69.73 % at t:72 h. Consequently, increasing the reaction time contributed positively to the formation of $SrTiO_3$.

Table 4.4. Density and mole conversion values of green body and sintered body, (green body reacted with altered reaction times at 120°C and 140°C).

Sample code	t(h)	T(°C)	Green body bulk density (g/cm^3)	Green body relative density (%)	Sintered body bulk density by geometric (g/cm^3)	Sintered body bulk density by Archimedes (g/cm^3)	Mole conversion (%)
R1	6	120	1.99 (±0.01)	51.02 (±0.36)	2.99 (±0.12)	3.01 (±0.01)	40.80 (±1.22)
R2	24	120	2.09 (±0.01)	53.57 (±0.38)	3.80 (±0.23)	3.67 (±0.03)	58.90 (±1.84)
R3	72	120	1.97 (±0.03)	50.64 (±0.90)	3.75 (±0.24)	3.80 (±0.09)	68.87 (±0.76)
R4	6	140	1.96 (±0.05)	50.25 (±1.44)	3.45 (±0.13)	3.47 (±0.07)	55.82 (±3.21)

(Cont. on the next page.)

Table 4.4. Cont.

R5	24	140	2.03 (±0.02)	52.11 (±0.82)	3.50 (±0.11)	3.53 (±0.01)	56.70 (±1.12)
R6	72	140	2.01 (±0.04)	51.53 (±1.08)	3.62 (±0.09)	3.81 (±0.07)	69.73 (±2.34)

Theoretical density values of the pellets obtained in the rHLPD experiments performed at different reaction times are shown in Table 4.5. While the theoretical density value of the pellet, which was reacted at 120°C for 6 h, was 66.23 %, it reached 79.63 % in 72 h. Likewise, the theoretical density value of the pellet was reacted at 140°C for 6 h, was 74.63 %, it reached 79.42 % in 72 h. Consequently, final relative density values also increased with increasing reaction time, and the porosity in the sintered body decreased.

Table 4.5. Density and porosity values of rHLPD samples reacted at 120°C and 140°C for different reaction times.

Sample code	**Sintered body bulk density by Archimedes (g/cm^3)**	**Sintered body theoretical density (via ROM) (g/cm^3)**	**Final relative density ($\%\rho_{th}$)**	**Porosity (P) (vol%)**
R1 (120°C-6 h)	3.01 (±0.01)	4.48 (±0.11)	67.08 (±0.14)	32.91 (±0.14)
R2 (120°C-24 h)	3.67 (±0.03)	4.75 (±0.02)	77.90 (±0.90)	22.10 (±0.90)
R3 (120°C-72 h)	3.80 (±0.09)	4.83 (±0.04)	79.73 (±1.50)	20.26 (±1.50)
R4 (140°C-6 h)	3.47 (±0.07)	4.66 (±0.09)	74.68 (±0.72)	25.31 (±0.72)

(Cont. on the next page.)

Table 4.5.Cont.

R5 (140°C-24 h)	3.53 (±0.01)	4.70 (±0.04)	73.27 (±2.60)	26.73 (±2.60)
R6 (140°C-72 h)	3.81 (±0.07)	4.81 (±0.07)	79.43 (±0.31)	20.57 (±0.31)

Figure 4.5(a) and 4.6(a) shows XRD patterns of experiments carried out at 120°C and 140°C at different reaction times. According to the XRD analysis of the $SrTiO_3$ pellets, ICDD No # 01-071-1166 TiO_2 remained in the structure. There were ICDD No # 01-073-0661 $SrTiO_3$ and ICDD No # 01-071-1166 TiO_2 in all experiments in the general structure.

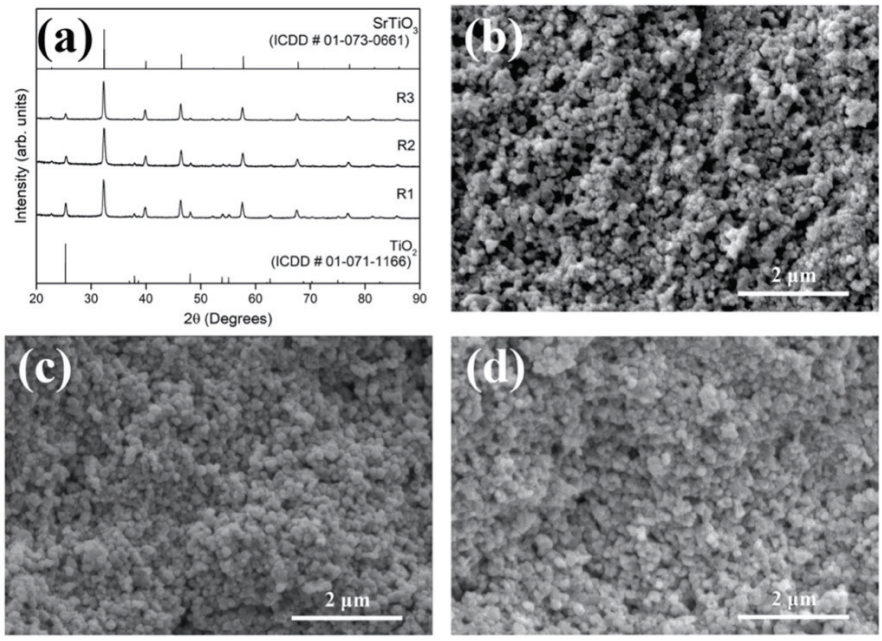

Figure 4.5. (a) XRD pattern of samples obtained at different reaction times at 120°C; SEM micrographs of fracture surface of samples; (b) R1 (6 h), (c) R2 (24 h), and (d) R3 (72 h). ICDD database for TiO_2 (ICDD # 01-071-1166), and $SrTiO_3$ (ICDD # 01-073-0661) are also included in the figures.

Figure 4.5 (b-d) and Figure 4.6 (b-d) illustrate SEM micrographs from fracture surfaces of samples for different reaction times. It is seen that the porous TiO_2 green bodies turned into relatively densified samples. R3 sample reacted in 72 h was better densified than R1 and R2 samples at 6 h and 24 h, respectively.

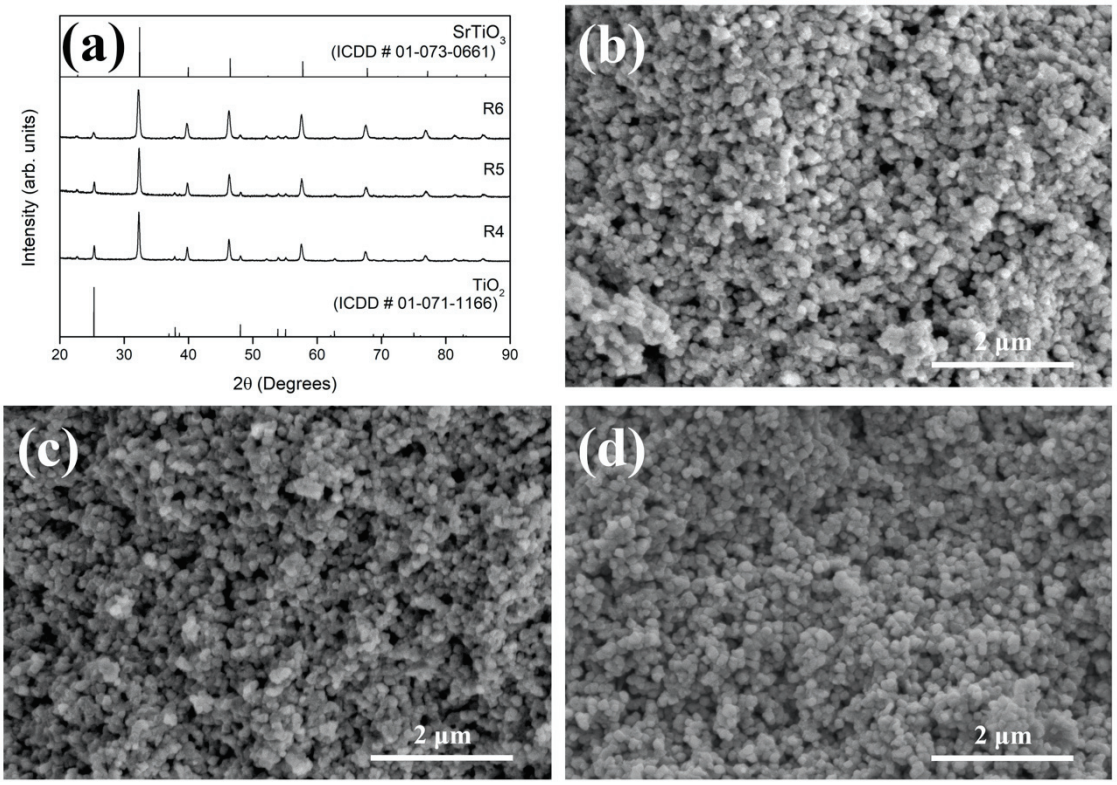

Figure 4.6. (a) XRD pattern of samples obtained at different reaction times at 140°C; SEM micrographs of fracture surface of samples (b) R4 (6 h), (c) R5 (24 h), and (d) R6 (72 h). ICDD database for TiO_2 (ICDD # 01-071-1166), and $SrTiO_3$ (ICDD # 01-073-0661) are also included in the figures.

As time progressed, both at 120°C and 140°C, the peak intensities of the anatase phase decreased, while the peak intensity of the $SrTiO_3$ phase increased. This illustrates that strontium hydroxide and TiO_2 react to form $SrTiO_3$.

FTIR analysis was performed to determine the chemical bonds in the structure of six samples carried out at different times. Figure 4.7 shows the FTIR spectrum of $SrTiO_3$-

TiO_2 ceramics. It indicates the presence of the hydroxyl group resulting from the peak OH stretch around 3400 cm^{-1}. The peak corresponding to approximately 400 cm^{-1} shows the Ti-O bending vibrations. The peak corresponding to TiO_2 is around 550 cm^{-1}. The band showing the Sr-O bond is much more noticeable than the others, with the absorption peaks around 580 cm^{-1}.[17]

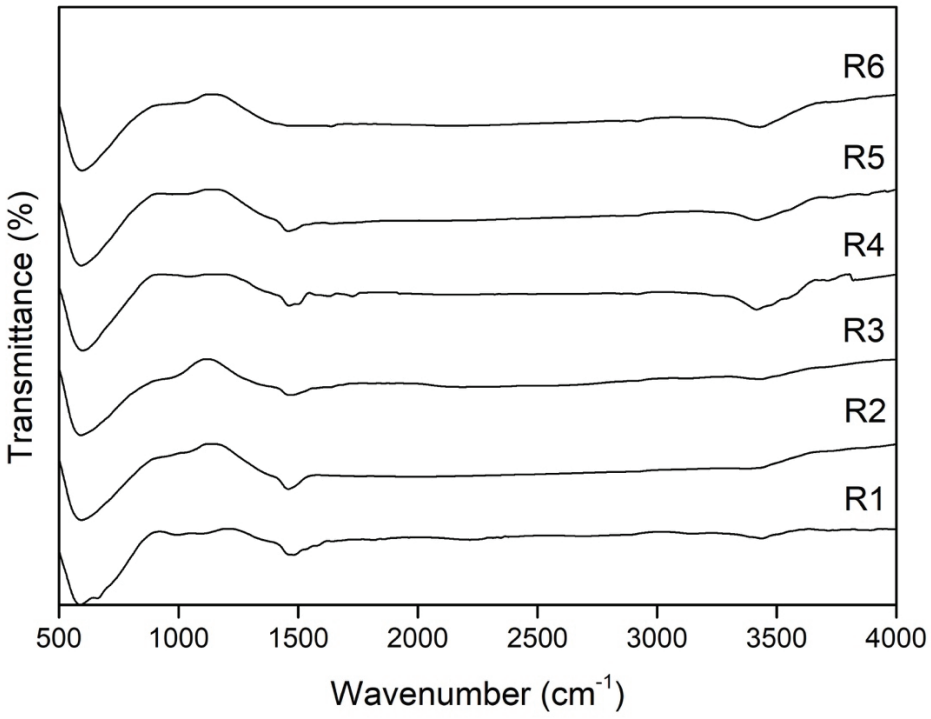

Figure 4.7. FTIR transmittance spectra of experiments for altered reaction times; R1: (120°C-6 h), R2: (120°C-24 h), R3: (120°C-72 h), R4: (140°C-6 h), R5: (140°C-24 h), and R6: (140°C-72 h).

4.5. Effect of Additional NaOH Concentration

In this experimental set, the optimum reaction temperature and reaction time were selected by looking at the results of the previous experiments. As in the reaction time experiments, T= 120-140°C and t= 24 h were determined.

The purpose of the addition of NaOH was to increase the reaction kinetics. In Table 4.6, the increase in mole conversion values was directly proportional to the increasing NaOH concentration. It shows that the reaction kinetics increased. In the experiments performed at 120 °C and 140°C, it is seen that the mole conversion increased as the NaOH concentration increased. This increase was thought to be due to the alkalinity increase with the addition of NaOH. In some studies in the literature, it was observed that the increase in alkalinity supported the formation of $SrTiO_3$.[57]

Table 4.6. Density and mole conversion values of green body and sintered body, (green body reacted with varying NaOH concentration for 24 h).

Sample code	NaOH (M)	t(h)	T(°C)	Green body bulk density (g/cm^3)	Green body relative density (%)	Sintered body bulk density by geometric (g/cm^3)	Sintered body bulk density by Archimedes (g/cm^3)	Mole conversion (%)
N1	0.1	24	120	2.02 (±0.02)	51.79 (±0.72)	3.34 (±0.12)	3.33 (±0.08)	58.60 (±1.98)
N2	0.5	24	120	2.00 (±0.04)	51.40 (±1.26)	3.41 (±0.09)	3.59 (±0.10)	68.73 (± 2.21)
N3	1	24	120	1.99 (±0.02)	51.14 (±0.54)	3.72 (±0.05)	3.84 (±0.06)	69.12 (± 3.65)
N4	0.1	24	140	2.01 (±0.03)	51.66 (±0.90)	3.30 (±0.07)	3.47 (±0.09)	55.70 (± 2.32)
N5	0.5	24	140	2.04 (±0.01)	52.30 (±0.36)	3.55 (± 0.09)	3.63 (±0.04)	61.42 (± 1.56)
N6	1	24	140	2.01 (±0.02)	51.66 (±0.54)	3.69 (±0.05)	3.67 (±0.03)	65.21 (± 1.73)

The final relative density values of the pellets obtained in the rHLPD experiments performed at altered NaOH concentration are shown in Table 4.7. While the final relative density value of the pellet, which reacted with the addition of 0.1 M NaOH at 120°C, was 71.22 %, it reached 81.55 % at 1 M. Likewise, the final relative density value of the pellet increased from 72.09 % of the sample reacted with the addition of 0.1 M NaOH at 140°C to 75.73 % at 1 M. As a result, the final relative density values also increased with increasing NaOH concentration and the porosity in the sintered body decreased.

Table 4.7. Density and porosity values of rHLPD samples reacted with altered NaOH concentrations at 120°C and 140°C for 24 h.

Sample code	**Sintered body bulk density by Archimedes (g/cm^3)**	**Sintered body theoretical density (via ROM) (g/cm^3)**	**Final relative density ($\%\rho_{th}$)**	**Porosity (P) (vol%)**
N1 (120°C-0.1 M)	3.33 (±0.08)	4.78 (±0.03)	70.32 (±0.91)	29.68 (±0.91)
N2 (120°C- 0.5 M)	3.59 (±0.10)	4.87 (±0.02)	74.86 (±1.61)	25.14 (±1.61)
N3 (120°C- 1 M)	3.84 (±0.06)	4.82 (±0.07)	81.21 (±2.18)	18.78 (±2.18)
N4 (140°C- 0.1 M)	3.47 (±0.09)	4.71 (±0.02)	72.50 (±1.80)	27.49 (±1.80)
N5 (140°C- 0.5 M)	3.63 (±0.04)	4.74 (±0.06)	75.46 (±1.58)	24.54 (±1.58)
N6 (140°C- 1 M)	3.67 (±0.03)	4.83 (±0.02)	77.31 (±1.88)	22.68 (±1.88)

The XRD analysis of the samples reacted under different NaOH concentration conditions at 120 ºC and 140ºC are shown in Figure 4.8. According to the XRD patterns of the experiments performed at different NaOH concentrations, ICDD No # 01-071-1166 TiO_2 remained in the structure. There were ICDD No # 01-073-0661 $SrTiO_3$ and ICDD No # 01-071-1166 TiO_2 in all experiments in the general structure.

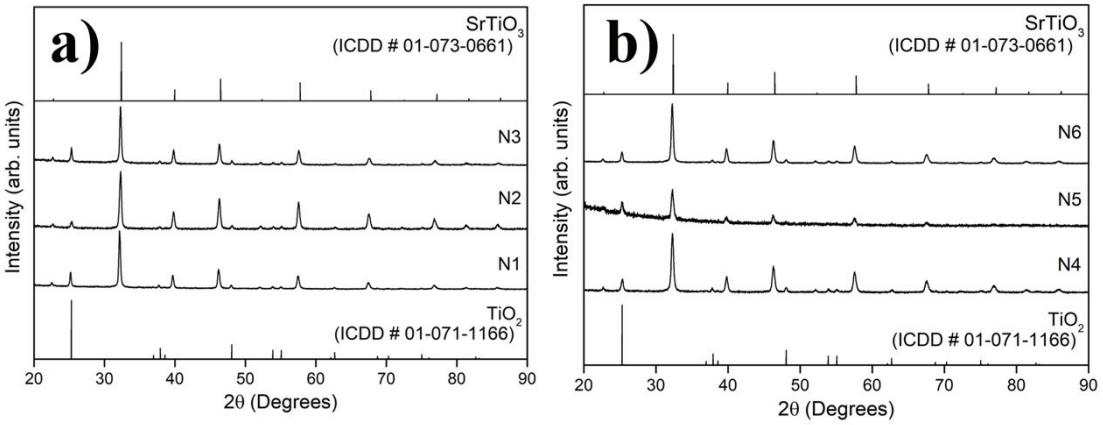

Figure 4.8. XRD analysis of samples produced with altered NaOH concentrations; (a) 120ºC (N1: 0.1 M / N2: 0.5 M / N3: 1 M), and (b) 140ºC (N4: 0.1 M / N5: 0.5 M / N6: 1 M). ICDD database for TiO_2 (ICDD # 01-071-1166), and $SrTiO_3$ (ICDD # 01-073-0661) are also included in the figures.

CHAPTER 5

CONCLUSIONS

In this thesis, $SrTiO_3$ monolithic ceramics were produced by using the ceramic densification method called rHLPD. To begin with, TiO_2 powder was mixed with PVA solution for 24 h. Then, grinding, and sieving processes were carried out after the mixture was dried in the oven at 80°C. After sieving, TiO_2 powder was pressed into 10mm diameter discs. The binder burnout process was applied to TiO_2 green bodies for 5 h at 400°C. After preparing the TiO_2 porous matrix, water, and $Sr(OH)_2.8H_2O$ were mixed according to the experimental parameters to form strontium hydroxide solution. After mixing $Sr(OH)_2.8H_2O$ and distilled water in a magnetic stirrer, water was added to reach the final volume of 70 %. Then the prepared solution was first used for pre-infiltration of the binderless porous matrix. After the binderless green body was infiltrated with the prepared solution, the TiO_2 green body and the hydroxide solution were poured into Teflon. Finally, the hydrothermal reaction was performed with different temperature and time parameters.

The microstructural and phase analysis of each experimental set was carried out by SEM and XRD analysis. The effect of each parameter on the final product was examined. The structure consisted of $SrTiO_3$ and TiO_2, and no $SrCO_3$ phase was observed based on XRD analysis. According to the experiments at different reaction temperatures made for monolithic $SrTiO_3$ production, it was seen that the most suitable temperatures were 120°C and 140°C. In the experiments, it was observed that the mole conversion value was 58.90 % at 120°C-24 h (T2) and 56.70 % at 140°C-24 h (T3). Accordingly, while the relative density of the green body was 53.57 %, the final relative density value of the T2 sample reached 77.90 %. The temperature increases from 90°C to 120°C stimulated the reaction to take place. As the temperature continued to increase, the mole conversion values began to decrease. After the experiments were carried out at different reaction temperatures, experiments were performed at various reaction times at 120°C and 140°C. Experiments were done from 6 to 72 h. As a result of those experiments, the increase in reaction time (at 120°C and 140°C) increased the mole conversion and the

final relative density value. Increasing the reaction time supported the formation of $SrTiO_3$. While the mole conversion was 40.80 % at 120°C for 6 h experiment, it was 68.87 % for 72 h. In addition, when the reaction time increased from 6 h to 72 h at 120°C, the final relative density value increased from 67.08 % to 79.73 %. Similarly, mole conversion at 140°C was 55.82 % for 6 h, while it was 69.73 % for 72 h. When the reaction time rose from 6 to 72 h at 140°C, the final relative density value was 79.43 %. In the experiments with NaOH, it was viewed that the NaOH solution increased the alkalinity and triggered the formation of $SrTiO_3$. With the addition of 1 M NaOH, the final relative density value reached 81.21 % at 120°C.

According to all those results, monolithic $SrTiO_3[TiO_2]$ ceramic composites were produced by the rHLPD method.

REFERENCES

1. Vakifahmetoglu, C.; Karacasulu, L., Cold sintering of ceramics and glasses: A review. *Current Opinion in Solid State and Materials Science* **2020,** *24* (1), 100807.
2. Chandler, C. D.; Roger, C.; Hampden-Smith, M. J., Chemical aspects of solution routes to perovskite-phase mixed-metal oxides from metal-organic precursors. *Chemical reviews* **1993,** *93* (3), 1205-1241.
3. Patwardhan, S.; Cao, D. H.; Hatch, S.; Farha, O. K.; Hupp, J. T.; Kanatzidis, M. G.; Schatz, G. C., Introducing perovskite solar cells to undergraduates. ACS Publications: 2015.
4. Galasso, F. S., *Structure, properties and preparation of perovskite-type compounds: international series of monographs in solid state physics*. Elsevier: 2013; Vol. 5.
5. Nikonov, A.; Kuterbekov, K.; Bekmyrza, K. Z.; Pavzderin, N., A brief review of conductivity and thermal expansion of perovskite-related oxides for SOFC cathode. *Eurasian Journal of Physics and Functional Materials* **2018,** *2* (3), 274-292.
6. Moon, J.; Kerchner, J. A.; Krarup, H.; Adair, J. H., Hydrothermal synthesis of ferroelectric perovskites from chemically modified titanium isopropoxide and acetate salts. *Journal of materials research* **1999,** *14* (2), 425-435.
7. Abrahams, S.; Keve, E., Structural basis of ferroelectricity and ferroelastcity. *ferroelectrics* **1971,** *2* (1), 129-154.
8. Dehkordi, A. M., An Experimental Investigation Towards Improvement of Thermoelectric Properties of Strontium Titanate Ceramics. *ProQuest Dissertations and Theses* **2014**, 76-02.
9. Sun, J.; Gao, T.; Song, X.; Zhao, Y.; Lin, Y.; Wang, H.; Ma, D.; Chen, Y.; Xiang, W.; Wang, J., Direct growth of high-quality graphene on high-κ dielectric SrTiO3 substrates. *Journal of the American Chemical Society* **2014,** *136* (18), 6574-6577.
10. Zhan, H.; Chen, Z.-G.; Zhuang, J.; Yang, X.; Wu, Q.; Jiang, X.; Liang, C.; Wu, M.; Zou, J., Correlation between multiple growth stages and photocatalysis of SrTiO3 nanocrystals. *The Journal of Physical Chemistry C* **2015,** *119* (7), 3530-3537.
11. Fang, X., Phase Transitions in Strontium Titanate. *Department of Physics, University of Illinois at Urbana-Champaign* **2013**.

12. Kalyani, V.; Vasile, B. S.; Ianculescu, A.; Buscaglia, M. T.; Buscaglia, V.; Nanni, P., Hydrothermal synthesis of SrTiO3 mesocrystals: single crystal to mesocrystal transformation induced by topochemical reactions. *Crystal growth & design* **2012,** *12* (9), 4450-4456.

13. Phoon, B. L.; Lai, C. W.; Juan, J. C.; Show, P. L.; Chen, W. H., A review of synthesis and morphology of SrTiO 3 for energy and other applications. *International Journal of Energy Research* **2019,** *43* (10), 5151-5174.

14. Bussmann-Holder, A.; Büttner, H.; Bishop, A., Stabilization of ferroelectricity in quantum paraelectrics by isotopic substitution. *Journal of Physics: Condensed Matter* **2000,** *12* (6), L115.

15. Gillani, S.; Ahmad, R.; Rizwan, M.; Shakil, M.; Rafique, M.; Murtaza, G.; Jin, H., First-principles investigation of structural, electronic, optical and thermal properties of Zinc doped SrTiO3. *Optik* **2020,** *201*, 163481.

16. Pai, Y.-Y.; Tylan-Tyler, A.; Irvin, P.; Levy, J., Physics of SrTiO3-based heterostructures and nanostructures: a review. *Reports on Progress in Physics* **2018,** *81* (3), 036503.

17. Viruthagiri, G.; Praveen, P.; Mugundan, S.; Gopinathan, E., Synthesis and characterization of pure and nickel doped SrTiO3 nanoparticles via solid state reaction route. *Ind. J. Adv. Chem. Sci* **2013,** *1*, 132-138.

18. West, A. R., *Solid state chemistry and its applications*. John Wiley & Sons: 2014.

19. Athayde, D. D.; Souza, D. F.; Silva, A. M.; Vasconcelos, D.; Nunes, E. H.; da Costa, J. C. D.; Vasconcelos, W. L., Review of perovskite ceramic synthesis and membrane preparation methods. *Ceramics International* **2016,** *42* (6), 6555-6571.

20. Kingery, W. D.; Bowen, H. K.; Uhlmann, D. R., *Introduction to ceramics*. John wiley & sons: 1976; Vol. 17.

21. Stojanovic, B. D.; Dzunuzovic, A. S.; Ilic, N. I., Review of methods for the preparation of magnetic metal oxides. In *Magnetic, Ferroelectric, and Multiferroic Metal Oxides*, Elsevier: 2018; pp 333-359.

22. Youssef, A.; Farag, H.; El-Kheshen, A.; Hammad, F., Synthesis of nano-structured strontium titanate by sol-gel and solid state routes. *Silicon* **2018,** *10* (3), 1225-1230.

23. Rabuffetti, F. A.; Kim, H.-S.; Enterkin, J. A.; Wang, Y.; Lanier, C. H.; Marks, L. D.; Poeppelmeier, K. R.; Stair, P. C., Synthesis-dependent first-order Raman

scattering in SrTiO3 nanocubes at room temperature. *Chemistry of Materials* **2008,** *20* (17), 5628-5635.

24. Zhang, J.; Huang, M.; Yanagisawa, K.; Yao, S., NaCl–H2O-assisted preparation of SrTiO3 nanoparticles by solid state reaction at low temperature. *Ceramics International* **2015,** *41* (4), 5439-5444.

25. Trabelsi, H.; Bejar, M.; Dhahri, E.; Graça, M.; Valente, M.; Khirouni, K., Structure, Raman, dielectric behavior and electrical conduction mechanism of strontium titanate. *Physica E: Low-dimensional Systems and Nanostructures* **2018,** *99*, 75-81.

26. Wang, D.; Ye, J.; Kako, T.; Kimura, T., Photophysical and photocatalytic properties of SrTiO3 doped with Cr cations on different sites. *The Journal of Physical Chemistry B* **2006,** *110* (32), 15824-15830.

27. Moos, R.; Härdtl, K. H., Dependence of the intrinsic conductivity minimum of SrTiO3 ceramics on the sintering atmosphere. *Journal of the American Ceramic Society* **1995,** *78* (9), 2569-2571.

28. Coonrod, S. S., Solid State Synthesis of the SrTiO3 Nano-particle. **2014**.

29. Yan, L. C.; Hassan, J.; Hashim, M.; Yin, W. S.; Khoon, T. F.; Jeng, W. Y., Effect of sintering temperatures on the microstructure and dielectric properties of SrTiO3. *World Appl Sci J* **2011,** *15*, 1614-1618.

30. Wang, Z.; Cao, M.; Yao, Z.; Li, G.; Song, Z.; Hu, W.; Hao, H.; Liu, H.; Yu, Z., Effects of Sr/Ti ratio on the microstructure and energy storage properties of nonstoichiometric SrTiO3 ceramics. *Ceramics International* **2014,** *40* (1), 929-933.

31. Silva, E. R.; Curi, M.; Furtado, J.; Ferraz, H.; Secchi, A., The effect of calcination atmosphere on structural properties of Y-doped SrTiO3 perovskite anode for SOFC prepared by solid-state reaction. *Ceramics International* **2019,** *45* (8), 9761-9770.

32. Liu, Y.; Xie, L.; Li, Y.; Yang, R.; Qu, J.; Li, Y.; Li, X., Synthesis and high photocatalytic hydrogen production of SrTiO3 nanoparticles from water splitting under UV irradiation. *Journal of Power Sources* **2008,** *183* (2), 701-707.

33. Wang, J.; Yin, S.; Komatsu, M.; Zhang, Q.; Saito, F.; Sato, T., Preparation and characterization of nitrogen doped SrTiO3 photocatalyst. *Journal of Photochemistry and Photobiology A: Chemistry* **2004,** *165* (1-3), 149-156.

34. Amaral, L.; Senos, A. M.; Vilarinho, P. M., Sintering kinetic studies in nonstoichiometric strontium titanate ceramics. *Materials Research Bulletin* **2009,** *44* (2), 263-270.

35. Abrantes, J.; Labrincha, J.; Frade, J., Applicability of the brick layer model to describe the grain boundary properties of strontium titanate ceramics. *Journal of the European Ceramic Society* **2000,** *20* (10), 1603-1609.

36. Trabelsi, H.; Bejar, M.; Dhahri, E.; Sajieddine, M.; Khirouni, K.; Prezas, P.; Melo, B.; Valente, M.; Graça, M., Effect of oxygen vacancies on SrTiO3 electrical properties. *Journal of Alloys and Compounds* **2017,** *723*, 894-903.

37. Sasaki, Y.; Nemoto, H.; Saito, K.; Kudo, A., Solar water splitting using powdered photocatalysts driven by Z-schematic interparticle electron transfer without an electron mediator. *The Journal of Physical Chemistry C* **2009,** *113* (40), 17536-17542.

38. Durán, A.; Martínez, E.; Díaz, J.; Siqueiros, J., Ferroelectricity at room temperature in Pr-doped Sr Ti O 3. *Journal of applied physics* **2005,** *97* (10), 104109.

39. Dai, Z.; Meiser, F.; Möhwald, H., Nanoengineering of iron oxide and iron oxide/silica hollow spheres by sequential layering combined with a sol–gel process. *Journal of colloid and interface science* **2005,** *288* (1), 298-300.

40. Malwal, D.; Packirisamy, G., Recent advances in the synthesis of metal oxide (MO) nanostructures. *Synthesis of Inorganic Nanomaterials* **2018**, 255-281.

41. Sakka, S., Chapter 11.1.2 - Sol–Gel Process and Applications. In *Handbook of Advanced Ceramics (Second Edition)*, Somiya, S., Ed. Academic Press: Oxford, 2013; pp 883-910.

42. Brinker, C. J.; Scherer, G. W., *Sol-gel science: the physics and chemistry of sol-gel processing*. Academic press: 2013.

43. Zhang, Z.; Zhao, L.; Wang, X.; Yang, J., The preparation and electrical properties of SrTiO 3-based capacitor-varistor double-function ceramics. *Journal of sol-gel science and technology* **2004,** *32* (1), 367-370.

44. Devi, A. D.; Sharma, H.; Sarma, H., Sol-gel processed strontium titanate ceramics. *Ferroelectric Letters* **2004,** *31* (3-4), 73-78.

45. Karoblis, D.; Diliautas, R.; Raudonyte-Svirbutaviciene, E.; Mazeika, K.; Baltrunas, D.; Beganskiene, A.; Zarkov, A.; Kareiva, A., The synthesis and characterization of sol-gel-derived SrTiO3-BiMnO3 solid solutions. *Crystals* **2020,** *10* (12), 1125.

46. Chen, L.; Zhang, S.; Wang, L.; Xue, D.; Yin, S., Preparation and photocatalytic properties of strontium titanate powders via sol–gel process. *Journal of crystal growth* **2009,** *311* (3), 746-748.

47. Pfaff, G., Sol–gel synthesis of strontium titanate powders of various compositions. *Journal of Materials Chemistry* **1993,** *3* (7), 721-724.

48. Byrappa, K.; Yoshimura, M., Handbook of hydrothermal technology, William Andrew. Elsevier: 2013.

49. Sōmiya, S.; Roy, R., Hydrothermal synthesis of fine oxide powders. *Bulletin of Materials Science* **2000,** *23* (6), 453-460.

50. Roy, R., Accelerating the kinetics of low-temperature inorganic syntheses. *Journal of Solid State Chemistry* **1994,** *111* (1), 11-17.

51. Riman, R. E.; Suchanek, W. L.; Lencka, M. M. In *Hydrothermal crystallization of ceramics*, Annales de Chimie Science des Materiaux, Elsevier: 2002; pp 15-36.

52. Kennedy, G. C., Pressure-volume-temperature relations in water at elevated temperatures and pressures. *American Journal of Science* **1950,** *248* (8), 540-564.

53. Morey, G. W., Hydrothermal synthesis. *Journal of the American Ceramic Society* **1953,** *36* (9), 279-285.

54. Ring, T. A., *Fundamentals of ceramic powder processing and synthesis*. Elsevier: 1996.

55. Piticescu, R.; Vilarnho, P.; Popescu, L.; Piticescu, R., Hydrothermal synthesis of perovskite based materials for microelectronic applications. *Journal of optoelectronics and advanced materials* **2006,** *8* (2), 543.

56. Dawson, W. J., Hydrothermal synthesis of advanced ceramic powders. *American Ceramic Society Bulletin* **1988,** *67* (10), 1673-1678.

57. Lencka, M. M.; Riman, R. E., Hydrothermal synthesis of perovskite materials: thermodynamic modeling and experimental verification. *Ferroelectrics* **1994,** *151* (1), 159-164.

58. Zhang, S.; Liu, J.; Han, Y.; Chen, B.; Li, X., Formation mechanisms of SrTiO3 nanoparticles under hydrothermal conditions. *Materials Science and Engineering: B* **2004,** *110* (1), 11-17.

59. Phoon, B. L.; Lai, C. W.; Pan, G.-T.; Yang, T. C.-K.; Juan, J. C., One-pot hydrothermal synthesis of strontium titanate nanoparticles photoelectrode using electrophoretic deposition for enhancing photoelectrochemical water splitting. *Ceramics International* **2018,** *44* (8), 9923-9933.

60. Zhang, H.; Zhu, Y.; Li, Z.; Fan, P.; Ma, W.; Xie, B., High discharged energy density of polymer nanocomposites containing paraelectric SrTiO3 nanowires for flexible energy storage device. *Journal of Alloys and Compounds* **2018,** *744*, 116-123.

61. Choi, J. Y.; Kim, C. H.; Kim, D. K., Hydrothermal synthesis of spherical perovskite oxide powders using spherical gel powders. *Journal of the American Ceramic Society* **1998,** *81* (5), 1353-1356.

62. Kobayashi, M.; Suzuki, Y.; Goto, T.; Cho, S. H.; Sekino, T.; Asakura, Y.; Yin, S., Low-temperature hydrothermal synthesis and characterization of SrTiO3 photocatalysts for NOx degradation. *Journal of the Ceramic Society of Japan* **2018,** *126* (2), 135-138.

63. Wu, G.; Li, P.; Xu, D.; Luo, B.; Hong, Y.; Shi, W.; Liu, C., Hydrothermal synthesis and visible-light-driven photocatalytic degradation for tetracycline of Mn-doped SrTiO3 nanocubes. *Applied Surface Science* **2015,** *333*, 39-47.

64. Huang, S.-T.; Lee, W. W.; Chang, J.-L.; Huang, W.-S.; Chou, S.-Y.; Chen, C.-C., Hydrothermal synthesis of SrTiO3 nanocubes: Characterization, photocatalytic activities, and degradation pathway. *Journal of the Taiwan Institute of Chemical Engineers* **2014,** *45* (4), 1927-1936.

65. Niishiro, R.; Tanaka, S.; Kudo, A., Hydrothermal-synthesized SrTiO3 photocatalyst codoped with rhodium and antimony with visible-light response for sacrificial H2 and O2 evolution and application to overall water splitting. *Applied Catalysis B: Environmental* **2014,** *150*, 187-196.

66. Souza, A.; Santos, G.; Barra, B.; Macedo Jr, W.; Teixeira, S.; Santos, C.; Senos, A.; Amaral, L.; Longo, E., Photoluminescence of SrTiO3: influence of particle size and morphology. *Crystal growth & design* **2012,** *12* (11), 5671-5679.

67. Lencka, M. M.; Riman, R. E., Thermodynamics of the hydrothermal synthesis of calcium titanate with reference to other alkaline-earth titanates. *Chemistry of materials* **1995,** *7* (1), 18-25.

68. Lencka, M. M.; Riman, R. E., Thermodynamic modeling of hydrothermal synthesis of ceramic powders. *Chemistry of Materials* **1993,** *5* (1), 61-70.

69. Chen, D.; Jiao, X.; Zhang, M., Hydrothermal synthesis of strontium titanate powders with nanometer size derived from different precursors. *Journal of the European Ceramic Society* **2000,** *20* (9), 1261-1265.

70. Wang, L.; Wang, Z.; Wang, D.; Shi, X.; Song, H.; Gao, X., The photocatalysis and mechanism of new SrTiO3/TiO2. *Solid state sciences* **2014,** *31*, 85-90.

71. Jayabal, P.; Sasirekha, V.; Mayandi, J.; Jeganathan, K.; Ramakrishnan, V., A facile hydrothermal synthesis of SrTiO3 for dye sensitized solar cell application. *Journal of alloys and compounds* **2014,** *586*, 456-461.

72. Mourão, H. A.; Lopes, O. F.; Ribeiro, C.; Mastelaro, V. R., Rapid hydrothermal synthesis and pH-dependent photocatalysis of strontium titanate microspheres. *Materials Science in Semiconductor Processing* **2015,** *30*, 651-657.

73. Da Silva, L. F.; Avansi, W.; Andrés, J.; Ribeiro, C.; Moreira, M. L.; Longo, E.; Mastelaro, V. R., Long-range and short-range structures of cube-like shape SrTiO 3 powders: microwave-assisted hydrothermal synthesis and photocatalytic activity. *Physical Chemistry Chemical Physics* **2013,** *15* (29), 12386-12393.

74. Yu, H.; Ouyang, S.; Yan, S.; Li, Z.; Yu, T.; Zou, Z., Sol–gel hydrothermal synthesis of visible-light-driven Cr-doped SrTiO 3 for efficient hydrogen production. *Journal of Materials Chemistry* **2011,** *21* (30), 11347-11351.

75. Avudaithai, M.; Kutty, T., Ultrafine powders of SrTiO3 from the hydrothermal preparation and their catalytic activity in the photolysis of water. *Materials research bulletin* **1987,** *22* (5), 641-650.

76. Tsumura, T.; Matsuoka, K.; Toyoda, M., Formation and annealing of BaTiO3 and SrTiO3 nanoparticles in KOH solution. *Journal of Materials Science & Technology* **2010,** *26* (1), 33-38.

77. Dong, W.; Li, X.; Yu, J.; Guo, W.; Li, B.; Tan, L.; Li, C.; Shi, J.; Wang, G., Porous SrTiO3 spheres with enhanced photocatalytic performance. *Materials Letters* **2012,** *67* (1), 131-134.

78. Joshi, U. A.; Lee, J. S., Template-free hydrothermal synthesis of single-crystalline barium titanate and strontium titanate nanowires. *Small* **2005,** *1* (12), 1172-1176.

79. He, G.-L.; Zhong, Y.-H.; Chen, M.-J.; Li, X.; Fang, Y.-P.; Xu, Y.-H., One-pot hydrothermal synthesis of SrTiO3-reduced graphene oxide composites with enhanced photocatalytic activity for hydrogen production. *Journal of Molecular Catalysis A: Chemical* **2016,** *423*, 70-76.

80. Crosby, L. A.; Chen, B.-R.; Kennedy, R. M.; Wen, J.; Poeppelmeier, K. R.; Bedzyk, M. J.; Marks, L. D., All roads lead to TiO2: TiO2-rich surfaces of barium and strontium titanate prepared by hydrothermal synthesis. *Chemistry of Materials* **2018,** *30* (3), 841-846.

81. Wang, Y.; Zhu, L.; Gao, F.; Xie, H. In *Preparation, characterization and photocatalytic activities of TiO2-SrTiO3 composites*, IOP Conference Series: Materials Science and Engineering, IOP Publishing: 2017; p 012038.

82. Kiss, B.; Manning, T. D.; Hesp, D.; Didier, C.; Taylor, A.; Pickup, D. M.; Chadwick, A. V.; Allison, H. E.; Dhanak, V. R.; Claridge, J. B., Nano-structured

rhodium doped SrTiO3–Visible light activated photocatalyst for water decontamination. *Applied Catalysis B: Environmental* **2017,** *206*, 547-555.

83. Zheng, Z.; Huang, B.; Qin, X.; Zhang, X.; Dai, Y., Facile synthesis of SrTiO3 hollow microspheres built as assembly of nanocubes and their associated photocatalytic activity. *Journal of colloid and interface science* **2011,** *358* (1), 68-72.

84. Grabowska, E.; Marchelek, M.; Klimczuk, T.; Lisowski, W.; Zaleska-Medynska, A., TiO2/SrTiO3 and SrTiO3 microspheres decorated with Rh, Ru or Pt nanoparticles: Highly UV–vis responsible photoactivity and mechanism. *Journal of Catalysis* **2017,** *350*, 159-173.

85. Lin, H.-y.; Cian, L.-T., Microwave-Assisted Hydrothermal Synthesis of SrTiO3: Rh for Photocatalytic Z-scheme Overall Water Splitting. *Applied Sciences* **2019,** *9* (1), 55.

86. Yu, H.; Wang, J.; Yan, S.; Yu, T.; Zou, Z., Elements doping to expand the light response of SrTiO3. *Journal of Photochemistry and Photobiology A: Chemistry* **2014,** *275*, 65-71.

87. Karaphun, A.; Hunpratub, S.; Swatsitang, E., Effect of annealing on magnetic properties of Fe-doped SrTiO3 nanopowders prepared by hydrothermal method. *Microelectronic engineering* **2014,** *126*, 42-48.

88. Zhang, Y.; Zhong, L.; Duan, D., Single-step hydrothermal synthesis of strontium titanate nanoparticles from crystalline anatase titanium dioxide. *Ceramics International* **2015,** *41* (10), 13516-13524.

89. Šetinc, T.; Spreitzer, M.; Vengust, D.; Jerman, I.; Suvorov, D., Inherent defects in sol-precipitation/hydrothermally derived SrTiO3 nanopowders. *Ceramics International* **2013,** *39* (6), 6727-6734.

90. Rangel-Hernandez, Y.; Rendón-Angeles, J.; Matamoros-Veloza, Z.; Pech-Canul, M.; Diaz-De La Torre, S.; Yanagisawa, K., One-step synthesis of fine SrTiO3 particles using SrSO4 ore under alkaline hydrothermal conditions. *Chemical Engineering Journal* **2009,** *155* (1-2), 483-492.

91. Sõmiya, S., Hydrothermal reactions for materials science and engineering: an overview of research in Japan. **2012**.

92. Guo, H.; Baker, A.; Guo, J.; Randall, C. A., Cold sintering process: a novel technique for low-temperature ceramic processing of ferroelectrics. *Journal of the American Ceramic Society* **2016,** *99* (11), 3489-3507.

93. Vakifahmetoglu, C.; Anger, J. F.; Atakan, V.; Quinn, S.; Gupta, S.; Li, Q.; Tang, L.; Riman, R. E., Reactive hydrothermal liquid-phase densification (rHLPD) of ceramics–A study of the BaTiO3 [TiO2] composite system. *Journal of the American Ceramic Society* **2016,** *99* (12), 3893-3901.

94. Li, H.-L.; Du, Z.-N.; Wang, G.-L.; Zhang, Y.-C., Low temperature molten salt synthesis of SrTiO3 submicron crystallites and nanocrystals in the eutectic NaCl–KCl. *Materials Letters* **2010,** *64* (3), 431-434.

95. Vendik, O.; Hollmann, E.; Kozyrev, A.; Prudan, A., Ferroelectric tuning of planar and bulk microwave devices. *Journal of Superconductivity* **1999,** *12* (2), 325-338.

96. Tkach, A.; Vilarinho, P.; Senos, A.; Kholkin, A., Effect of nonstoichiometry on the microstructure and dielectric properties of strontium titanate ceramics. *Journal of the European Ceramic Society* **2005,** *25* (12), 2769-2772.

97. Liu, X.; Bai, H., Liquid–solid reaction synthesis of SrTiO3 submicron-sized particles. *Materials Chemistry and Physics* **2011,** *127* (1-2), 21-23.

98. Adair, R.; Chase, L.; Payne, S. A., Nonlinear refractive index of optical crystals. *Physical Review B* **1989,** *39* (5), 3337.